LA-14098

Modern Fission Theory for Criticality

J. Eric Lynn

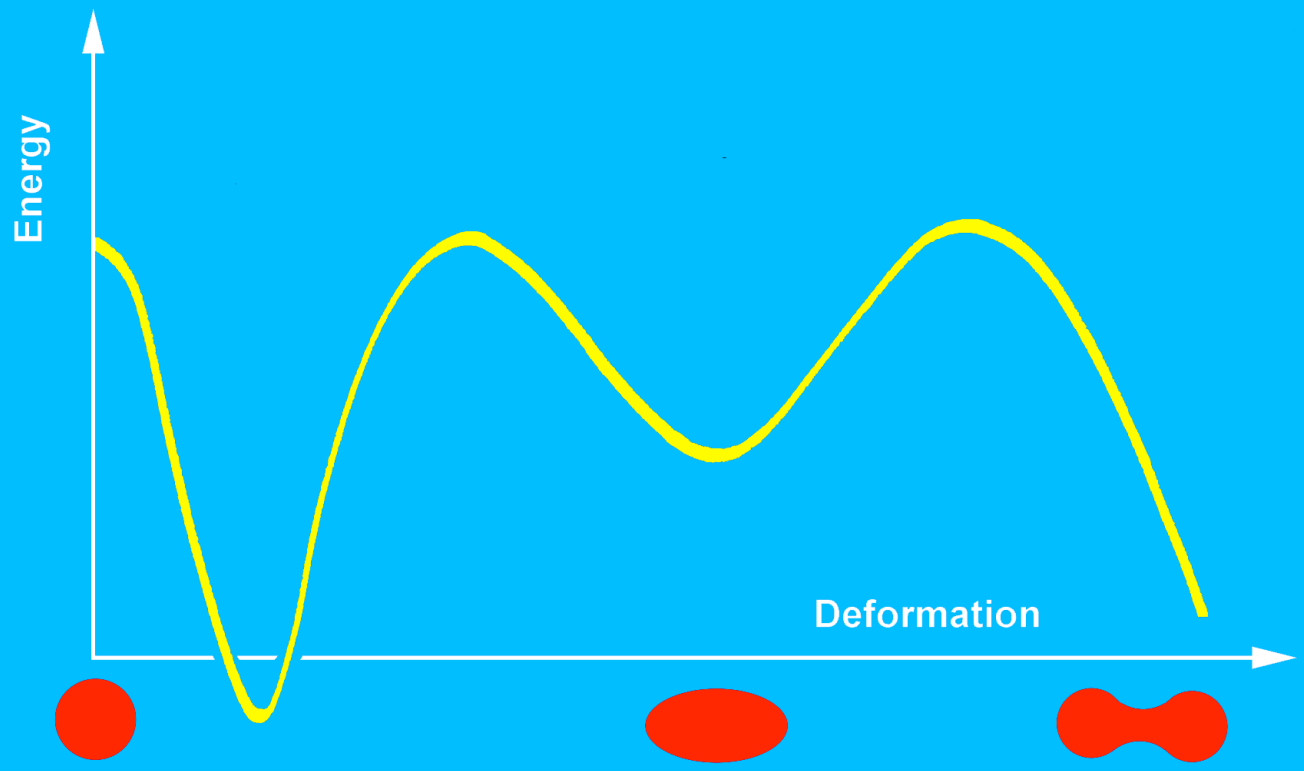

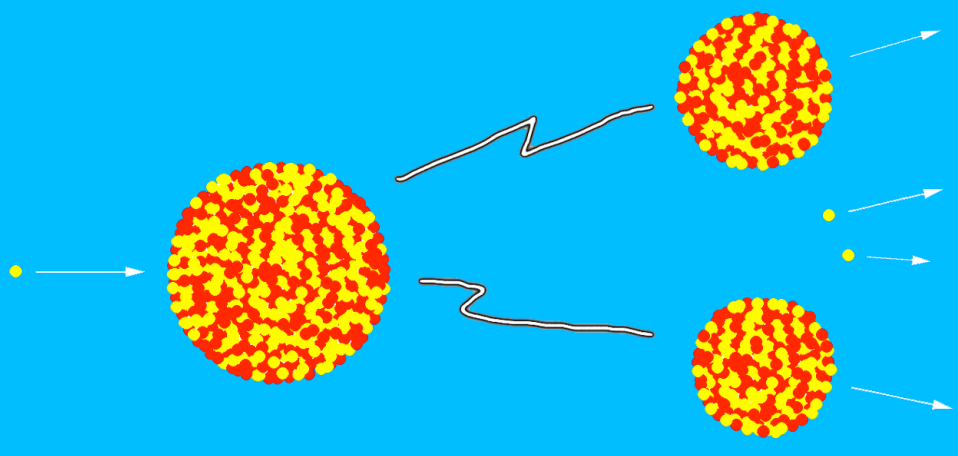

Los Alamos
NATIONAL LABORATORY

Composition and cover design *by Charles T. Rombough, CTR Technical Services, Inc.*

Printing coordination *by Jerry Halladay, Group IM-4*

LA-14098
Issued: February 2004

Modern Fission Theory for Criticality

J. Eric Lynn*

*Consultant at Los Alamos. Sumner Associates, Inc., 100 Cienega, Suite D, Santa Fe, NM, 87501-2236

Table of Contents

List of Figures

Foreword

In 1981 the American Nuclear Society published ANSI/ANS-8.15-1981, an American National Standard entitled *Nuclear Criticality Control of Special Actinide Elements*. In compliance with Society policy, the ANS-8.15 working group is in the process of reviewing and revising the Standard. Although Appendix A of the Standard, entitled "Criticality Aspects of Special Actinide Elements," is not formally part of the Standard, its relevance is recognized by the criticality safety community. As part of its efforts, the working group invited Dr. John Eric Lynn to give a presentation on the relevance and applicability of modern fission theory to Appendix A. That presentation is captured in this document.

Norman L. Pruvost
ANS-8.15 Working Group Chair

Acknowledgements

This review has been greatly improved and enhanced, chiefly by the enthusiasm and many suggestions of Norman L. Pruvost, Chairman of the ANS-8.15 Working Group. Charles T. Rombough has greatly contributed in the cover design, figure and text editing, and reference checking. Valuable input and comment has come from members of Thomas P. McLaughlin's HSR-6 Group at Los Alamos National Laboratory and from members of the ANS-8.15 Working Group.

Modern Fission Theory for Criticality

by

J. Eric Lynn

Abstract

Preparation of this document was inspired by the effort to revise American National Standard ANS-8.15, *Criticality Aspects of Special Actinide Elements*, dated 1981. Appendix A of ANS-8.15 is concerned with estimates of fissionability for actinides not included in the Standard. These estimates are based on a nuclear fission model published in 1958. In the present document, this model is subjected to critical analysis and discussion. It is found that its basis, an empirical relation of spontaneous fission half-lives to the fissility parameter of the liquid-drop theory leading to a relationship of the fission barrier and hence the neutron fission cross sections to the same parameter, is much too simplistic.

The current status of nuclear theory and its impact on fission theory is examined with the eventual aim of revising Appendix A for the revised Standard. The basis of the modern theory of fission is the interlocking of nuclear shell theory with the most modern versions of liquid-drop theory. We begin by reviewing nuclear shell phenomena and the theory for spherical nuclei. The theory is based on the notion of clustering of single-particle nucleon levels in a potential well, leading to energy gaps that give extra stability to certain nuclei — the closed shell or magic-number nuclei. The idea of single-particle levels in a potential well can be extended to deformed nuclei (these have nucleon numbers quite different from the magic numbers and are usually elongated — a spheroid in first approximation). Such deformed nuclei are also capable of forms of collective motion (vibrations and rotations). It is pointed out how these quantum states of nuclei that are deformed to the point at which they can overcome the fission barrier can affect the spontaneous fission half-lives and the fission cross sections in very specific ways. The basic development of the above work was mainly done in the 1950s.

The theories pioneered by Strutinsky, starting in the 1960s, are then described. These are based on the discovery that quasi-shell structure can occur in the sequences of single-particle levels as a function of elongation of the nucleus (or

indeed for other modes of deformation). The *relative* change in summed energies of the occupied single-particle levels can be added to the liquid-drop energy to give the total energy of the nucleus at a given deformation. In the actinides it is generally found that the total energy as a function of deformation goes through a double maximum with increasing elongation, i.e. the fission barrier is double humped. The often spectacular consequences of such a barrier are described, with special mention of spontaneously fissioning isomers, intermediate structure (a second class of resonance structure) in fission cross sections, and effect on the gross magnitude of the fission barrier height. The effects and importance of other modes of nuclear deformation (such as mass asymmetric and axially asymmetric deformations) are briefly reviewed.

The capability of this modern theory of fission to give estimates of fission and capture cross sections is then discussed. It is shown how data from reactions induced by particles other than neutrons can be used to obtain information on fission barrier properties of nuclei for which neutron cross-section measurements are limited are unavailable. Interpolation or extrapolation of barrier properties, guided by nuclear energy calculations of barrier trends, can lead to fission cross-section estimates of yet more nuclei. Examples of such calculations are presented.

I. Introduction

Nuclear criticality safety standards for operating with the three major fissile nuclides (^{233}U, ^{235}U, and ^{239}Pu) are set in *American National Standard for Nuclear Criticality Safety in Operations with Fissionable Materials Outside Reactors*, ANSI/ANS-8.1-1998.[1] Safety standards for 14 other important fissile and fissionable nuclides are provided in another document, *American National Standard for Nuclear Criticality Control of Special Actinide Elements*, ANSI/ANS-8.15-1981.[2] These nuclides, ranging from ^{237}Np to ^{251}Cf, do not comprise a complete list of all possible nuclides that may become of criticality safety concern in the future. For this reason the document ANS-8.15 includes an Appendix (Appendix A). In this Appendix, the estimates of fissionability* and criticality of a wide range of additional nuclides is based on the nuclear fission model described in a single 1958 paper by Vandenbosch and Seaborg.[3] The apparent intent of the Appendix was only to provide simple qualitative guidance on the likelihood of fission for the 14 nuclides addressed therein. However, the Vandenbosch and Seaborg paper that served as the basis for the Appendix was already outmoded by subsequent developments in fission physics between 1958 and the issuance of ANSI/ANS-8.15-1981.

Briefly, Ref. 3 is based on some early liquid-drop model calculations of penetrability of the liquid-drop fission barrier combined with empirical observations of the dependence of spontaneous fission half-lives on the liquid-drop fissility parameter (Z^2/A) and even-odd character† of the fissioning nucleus. The resulting estimates of fission barrier height and even more so, of fission "activation" energy, are very crude. Our present-day knowledge and understanding of fission physics is far more sophisticated and detailed than that discussed in Ref. 3 and should be used for making the best estimates of fissionability in a possibly revised Appendix A.

Another key physics statement made in Appendix A is "the key to potential criticality is whether the nuclide contains an even or odd number of neutrons, *N*." This is very much a rule-of-thumb statement. Already one exception (^{232}U) is recorded in Table A-1 of Appendix A and others are known or can be expected. The even or odd neutron number of the nucleus is only one of many other physics

* In this document, *fissionability* means the likelihood of a nucleus to fission. The higher the fissionability, the larger is the potential for such a material to achieve criticality.

† In this context, *even-odd character* refers to the number of protons (Z) and number of neutrons (N) being even or odd integers.

characteristics that must be considered in making an estimate of the potential for criticality.

The purpose of the present paper is to review our present knowledge and understanding of fission physics and thus to illustrate how it can be used to greatly improve our estimates of fission cross sections, over the full neutron energy range from slow to fast, for nuclear species for which measurements are either inadequate or non-existent. We begin with an outline of the liquid-drop model, which provides the basic framework for the rest of our understanding. In the section following this, we critically review the methods used in Ref. 3 for estimating barrier heights and "activation" energies. Because Ref. 3 was the key to Appendix A, we go into this topic in some detail. We then proceed to describe the rich tapestry of experimental observation and theoretical insight that followed publication of Vandenbosch and Seaborg's paper in 1958.

II. The Liquid-Drop Model

Underlying all theoretical discussions of nuclear fission is the concept of the liquid drop. Stemming originally from Weizsacker's semi-empirical formula[4] describing nuclear mass and hence mass defect or binding energy, E_B as a function of mass number A* is given as follows:

$$E_B = -c_V A + c_S A^{2/3} + c_C (Z^2/A^{1/3}) \pm \delta \quad (1)$$

This recognizes the principal terms respectively as equivalent to volume, surface, and Coulomb energy plus an even-odd fluctuation, δ. The coefficients c_V, c_S, c_C are established by fitting the mass-defect curve. This formula was enunciated by Meitner and Frisch[5] as the key to explaining the radiochemical discovery of nuclear fission by Hahn and Strassman,[6] and was then developed by Bohr and Wheeler[7] and their successors into a full-blown theory for fission.

The simple physical picture is that of surface energy resisting deformation from the spherical shape and the Coulomb energy promoting deformation towards an elongated spheroid. If the Coulomb energy is less than twice the surface energy then it costs energy to deform and the stable shape is spherical. But if energy is put in to force the drop to deform, then at a certain elongation the Coulomb forces overcome the surface tension and the drop becomes unstable to further elongation and ultimately splits into two smaller drops. The elongation at which this instability commences becomes greater as the ratio of Coulomb energy to surface energy becomes smaller. This ratio is known as the normalized fissility parameter, x:

$$x = E_C / 2E_S = (c_C / 2c_S)(Z^2/A) = (Z^2/A) / (Z^2/A)_{\text{crit}} \quad (2)$$

The normalized fissility parameter equals unity when

$$(Z^2/A)_{\text{crit}} = 2c_S/c_C \quad (3)$$

and at this value, the sphere is at unstable equilibrium.

Of course the shape of the liquid drop does not have to be a spheroid, and indeed beyond small deformations, the minimum energy shape at a given elongation is not

* In this document, A refers to the mass number which is the sum of the proton number, Z, and the neutron number, N, all three being integers.

a spheroid. The shape can be generalized by use of a multitude of parameters to describe it. One of the earliest sets comprised the coefficients of a representation of the surface as an expansion in Legendre polynomials. In this the first order term is the 2nd order polynomial P_2, describing quadrupole deformation, the spheroid, and its coefficient is denoted by β_2. Because this remains such an important term up to the instability point (at least for actinides and higher charge nuclides), it is generally used to denote the fission deformation variable (usually abbreviated to just β). However, other terms must be included. The hexadecapole term $\beta_4 P_4$ is certainly one of these. This term describes "necking-in" of the distorted drop. It follows that the liquid-drop potential energy must be calculated for a range of several of these variables. See Figure 1.

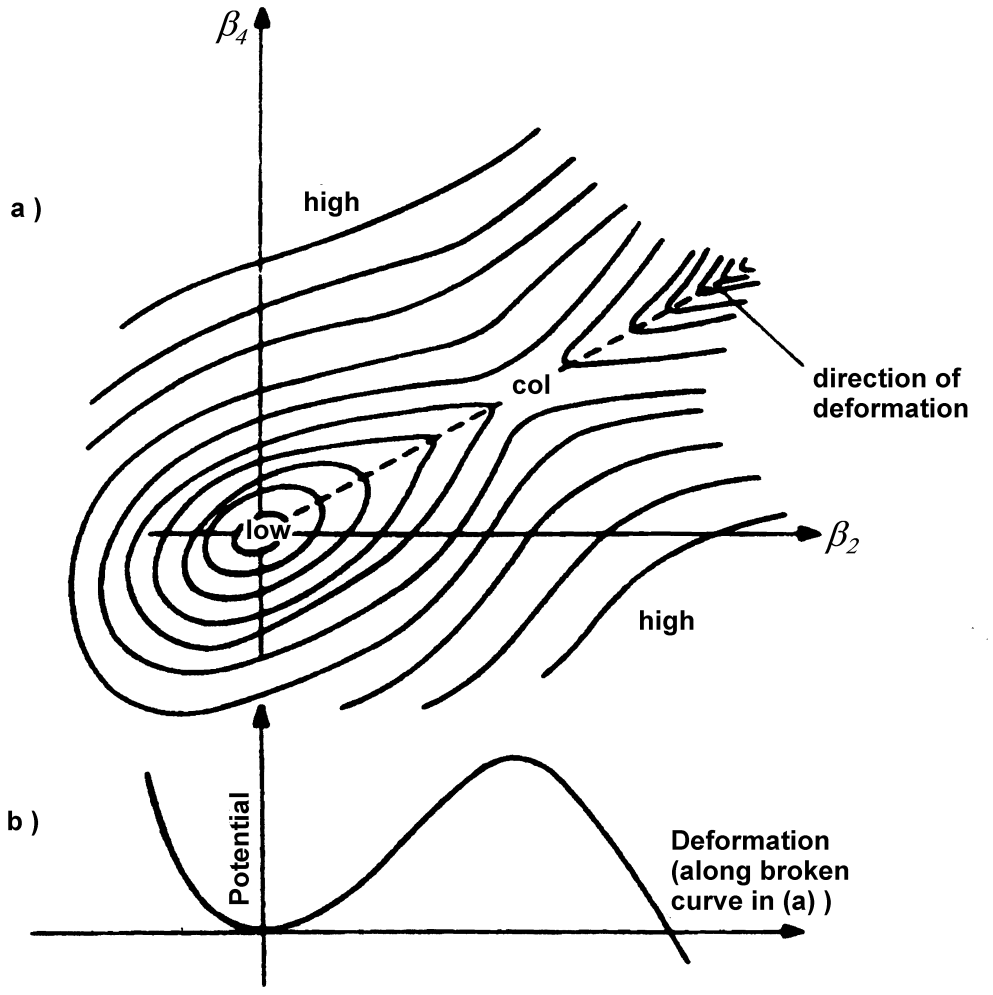

Figure 1. Schematic contours of liquid-drop energy as a function of two principal deformation parameters. Note: The figure (b) above is the energy on the least path (the fission barrier) which is the dashed line in (a). Adapted from Fig. 3 of Ref. 7.

The maximum in the minimum energy path to fission (this is the saddle point, denoted by **col**[*], in the potential energy diagram) marks the onset of instability to further elongation. The one-dimensional representation (Figure 1b) of the fission barrier is commonly used in discussions of fission.

III. The Fission Model in the Current Version of Appendix A

Appendix A of ANS-8.15 is apparently based partly on the liquid-drop model. The key reference is Vandenbosch and Seaborg.[3] The first part of this paper is an attempt to obtain a global equation for fission barrier heights and, hence, for fission "activation" energies. It bases quantitative estimates of barrier height on the papers of Frankel and Metropolis[8] and Seaborg.[9] The second part of the paper is concerned with obtaining average[†] values of the neutron width to fission width ratio at high excitation energies from (α,4n) reactions and is irrelevant to the problem of barrier heights. In the addendum to this report all the references given in Ref. 3 are surveyed and the relevance of each to the barrier height problem is noted.

The Frankel and Metropolis paper[8] gives liquid-drop model computations of barrier height and also calculates the quantal penetrability, using hydrodynamical estimates of the inertial tensor based on irrotational flow, for deforming through the barrier for a range of excitation energies. The calculations were done for the normalized fissility parameter $x = 0.74$ (appropriate for ^{238}U). From these they obtain a formula for the dependence of spontaneous fission half-life on the difference between barrier height V and excitation energy E:

$$\tau_{SF} = 3\times10^{-29}\times10^{7.85(V-E)} \text{ yr} = 10^{-21}\times10^{7.85(V-E)} \text{ sec} \qquad (4)$$

Seaborg[9] builds on an earlier paper (Ref. 10) to obtain an empirical dependence of τ_{SF} on Z^2/A:

$$\text{Log}_{10}\,\tau_{SF} \text{ (in yr)} = 149.5 - 3.75\,(Z^2/A) \qquad (5)$$

It has to be observed that this relationship applies only to even-even nuclides. Hindrance factors on the order of 10^3 to 10^5 apply to nuclides with odd numbers of nucleons. Seaborg's formula[9] for spontaneous fission dependence on Z^2/A was

[*] A French word meaning "mountain pass".
[†] In this discussion, "average" means the average value over all the resonances within a given energy interval.

obtained from the very limited and not very accurate data available 50 years ago. The greatly improved data base available today (see Ref. 11 and Figure 2) shows that (1) the values of the coefficients he obtained for Eq. 5 were somewhat ambiguous, because no unique straight line can be drawn through the data of Figure 2, and (2) the clusters of data for sets of isotopes of the same element shows that parameters other than Z^2/A are very important. Data points in Figure 2 can deviate as much as 15 orders of magnitude from Eq. 5. Much of this was recognized already in Ref. 3 but no changes were made to Eq. 5 in using it for deduction of fission activation energies.

By matching Eq. 5 to Eq. 4, Seaborg obtains an estimate for barrier height based on Z^2/A:

$$(22.7 - 0.477\ Z^2/A) \quad \text{MeV} \tag{6}$$

Seaborg then remarks that Eq. 4 from Ref. 9 only applies to ^{238}U. Extension to other values of Z^2/A leads to a more complicated expression. This is reasonable because we can expect the barrier "thickness" to depend on Z^2/A, but it is puzzling to know from where the results for other values of Z^2/A came. Frankel and Metropolis only made calculations for ^{238}U. But, no matter how the "extension to other values of Z^2/A" was obtained, his final expression for V_F is

$$(19 - 0.36\ Z^2/A) \quad \text{MeV} \tag{7}$$

This is compared with the Frankel and Metropolis' calculated liquid-drop barrier heights in Figure 3. Vandenbosch and Seaborg[3] add a final adjustment δ for the even-odd character of the nucleus. This is to bring the spontaneous fission half-lives of odd-neutron, odd-proton, and odd-odd nuclides into line with the relationship to barrier height. They find that $\delta = 0.4$ MeV for the odd-mass nuclides and $\delta = 0.7$ MeV for the odd-odd nuclides. The final formula for barrier height is

$$V_F = 19 - 0.36\ Z^2/A + \delta \quad \text{MeV} \tag{8}$$

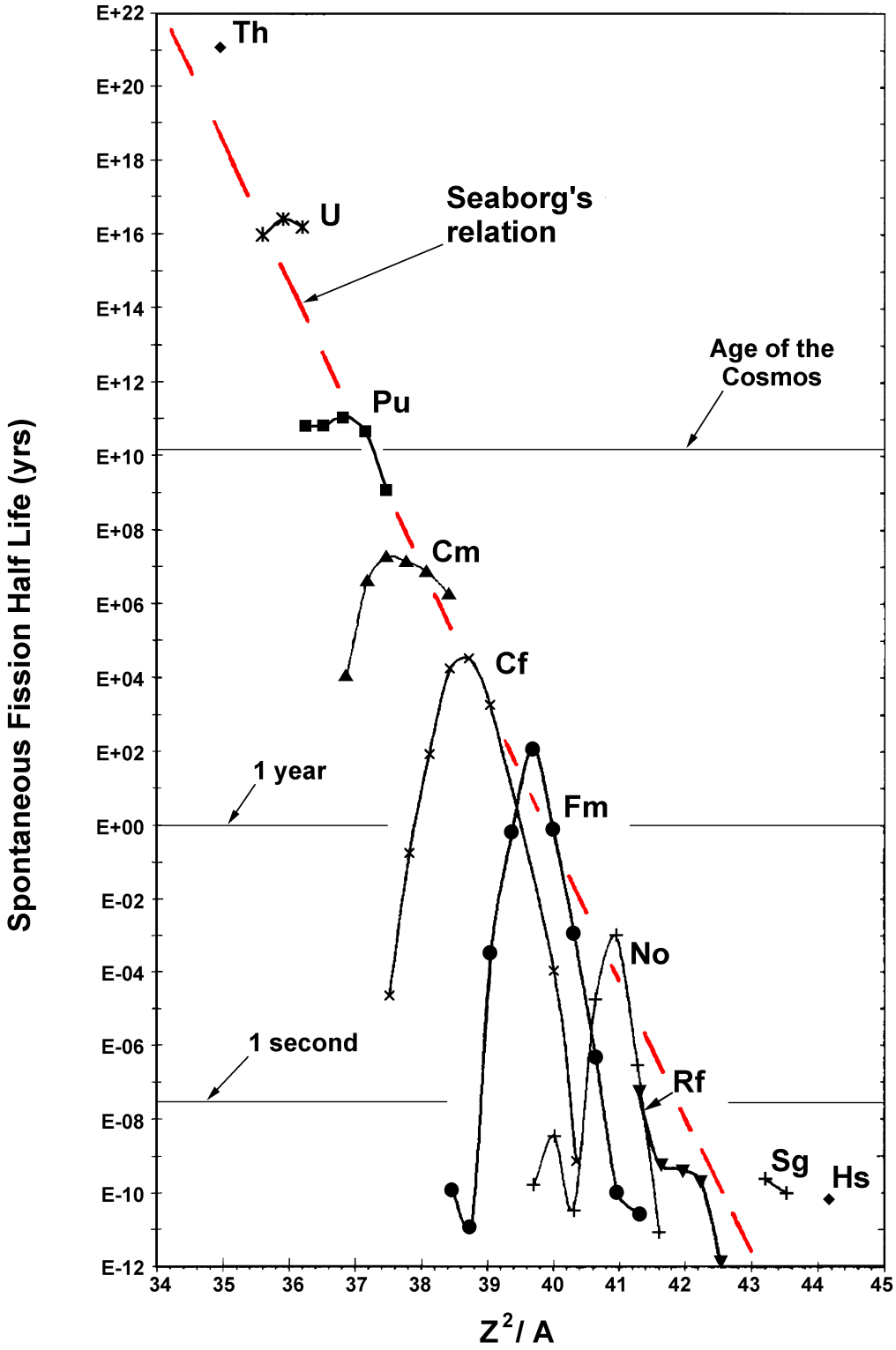

Figure 2. **Most recent compilation of data on spontaneous fission half-lives of even-even nuclei in the ground state.** Note: This data is taken from Ref. 11. The dashed red line is Seaborg's relation (Ref. 9). The author is indebted to John A. Miller of HSR-6, Los Alamos National Laboratory, for the construction of this graph.

We notice in Figure 3 that Eq. 7 (for even nuclides) from Ref. 9 is very different from the values of barrier height calculated by Frankel and Metropolis from the liquid-drop model. They only agree in the region of uranium ($Z^2/A \approx 36$), where they have been stitched together to obtain Eq. 7. Eq. 6 gives results for the barrier height that differ from Eq. 7 by deficits ranging from 0.35 MeV (^{226}Ra) to 0.85 MeV (^{242}Cm). The deficit is 0.45 MeV for ^{238}U. However, this adjustment is necessary in order to obtain better agreement between Eq. 4 and the observed spontaneous fission half-life of ^{238}U.

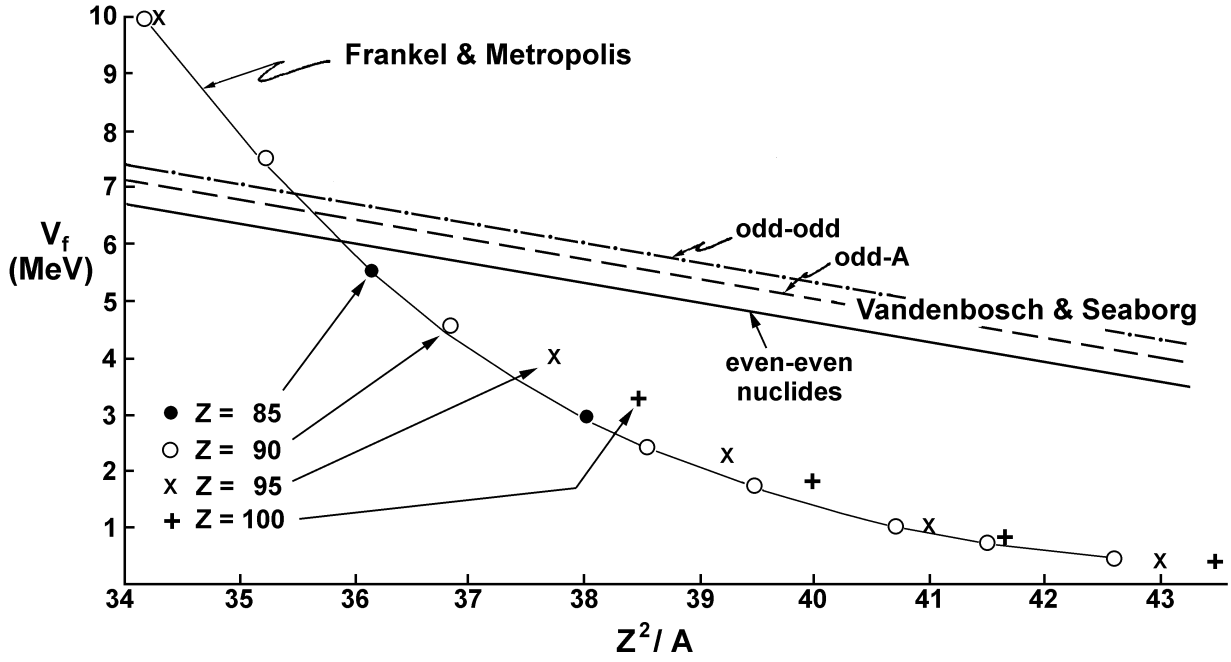

Figure 3. Comparison of Frankel and Metropolis liquid-drop calculations of fission barrier height with Vandenbosch and Seaborg's formula. Note: The indicated curve and symbols were extracted from data in Ref. 8. The V & S formula is from Ref. 3.

All this can be summarized by stating that Eq. 8 is an empirical deduction of barrier heights from spontaneous fission half-lives using a liquid-drop model calculation of barrier penetration. The latter has been calculated for the nucleus ^{238}U ($Z^2/A = 35.56$). There is no theoretical reason given in Ref. 3 or Ref. 9 for assuming that this penetrability factor is valid over a wide range of nuclides. The very fact that the liquid-drop model barriers differ so much from the empirical values demonstrates that the liquid-drop model cannot be used to support this assumption.

The fission half-life at the energy of the barrier is stated in Ref. 3 to be about 10^{-21} sec (see also Eq. 4). The "activation energy" is defined as the energy at which

the fission half-life equals the compound nucleus radiation decay half-life (10^{-14} sec). This is obtained from the barrier height by increasing the barrier half-life by the barrier penetration factor of Frankel and Metropolis, Eq. 4. The 10^7 increase required is equivalent to a reduction of 0.9 MeV below the fission barrier (see also Ref. 3). Thus, the fission "activation energy" is given by

$$E_A = V_F - 0.9 \text{ MeV} \tag{9}$$

According to Ref. 3, the difference between this and the neutron separation energy* appears to correlate well with "slow neutron fissionability," namely, that the thermal neutron fission cross section ($\sigma_{th,F}$) is greater than one barn. However, this definition is rather arbitrary. For criticality purposes, a better choice might have been that the ratio of the thermal fission and capture cross sections ($\sigma_{th,F} / \sigma_{th,\gamma}$) is greater than one.

An inconsistency in the procedure of the last paragraph derives from the statement that the fission half-life at the barrier is 10^{-21} sec. This is only true in the very general sense of unspecified decay of an excitation mode of very simple character (e.g., a pure vibrational mode or an independent particle state). Such modes have spacing on the order 1 to 10 MeV. The compound nucleus states that we are actually discussing here, and which have the radiation decay half-life of order 10^{-14} sec, have spacing on the order of 10 to 100 eV. This reduces the unhindered fission life from 10^{-21} sec to about 10^{-16} sec and consequently raises the fission activation energy on the above definition by about 0.6 MeV. This destroys much of the correlation with slow neutron fissionability reported in Ref. 3.

All of the above shows that the Vandenbosch and Seaborg formula is really empiricism and not the liquid-drop model, even though it contains Z^2/A, the variable that occurs in the liquid-drop model expression for the normalized fissility parameter, Eq. 2. Obtaining these global estimates of barrier heights was very important in the 1950s but they have now been superseded by the huge amount of knowledge on fission that has been gained since then. It is interesting to note that Ref. 3 is not mentioned at all in Vandenbosch and Huizenga's 1973 book on Nuclear Fission.[12]

* The *neutron separation energy* is the same as the binding energy of the last neutron in the nucleus.

So what changed between 1958 and 1973?

In fact there was a whole new set of startling phenomena observed in fission and a whole new platform was added to our theoretical understanding of the fission process.

Before describing these, we must go back in time and say something about relevant developments in nuclear structure modeling before 1958, which were not considered in the Vandenbosch and Seaborg paper.

IV. Developments in Nuclear Structure Theory (pre-1958)

1. **The shell model**

   This is based on the observation that "magic number" nuclei are especially stable (the binding energy is greater than the liquid-drop estimate — see Figure 4). The level spectra of near magic number nuclei are explained as level energies of single particles (neutrons or protons) in a spherical potential well with spin-orbit coupling. See Figure 5.

2. **The spherical shell model breaks down away from magic numbers**.

   Broad groups of nuclei, especially the rare earths and actinides, are found to have large quadrupole moments, thus indicating that they have a stable deformed shape.

3. **The even-even members of these large groups were found to exhibit *collective* behavior**.

   Their level spectra were interpreted by Bohr and Mottelson[13] as carrying quanta of vibrational and/or rotational energy. Later, the more complex spectra of non even-even nuclei were found to have these features as well.

4. **Extension of shell model type spectroscopy to deformed nuclei.**

   The energy levels of neutrons and protons are calculated as those of particles in a deformed potential well (Nilsson diagrams), Figures 6 and 7. These explained the spins and parities of ground states and (including rotational and vibrational bands) low-lying excited states. In Figures 6 and 7, the origin of the abscissa corresponds to the sphere and the ordinate shows the large energy gaps that appear in Figure 5. Each of the levels of the sphere is actually a degenerate subset. As elongation sets in, this degeneracy is broken and the spreading pattern of the Nilsson diagram appears.

   Two of the principal quantum numbers are parity and *projection* of the particle spin on the cylindrical symmetry axis of the deformed nucleus.

5. Pairing energy phenomena

a) **Even-even (e-e), even-odd (e-o)/odd-even (o-e), and odd-odd (o-o) discontinuities in binding energy**. The binding energy of the "last" neutron is greatest for an e-e nucleus and smallest for an o-o nucleus. Therefore, e-e is the most stable, o-o the least.

b**) "Energy gap" in level spectra of e-e nuclei.** This is a region in which only collective levels occur. In e-o/o-e nuclei this region contains only single-particle levels (spacing ~ 100 to 200 keV) with associated rotational bands. There is a much greater density in o-o nuclei (single-neutron + single-proton levels). This leads to the concept of paired particles occupying the same orbit, but with opposite spin, having correlated motion and attractive forces thus giving extra binding energy. A particle that is not bound in this correlated motion is known as a quasi-particle.

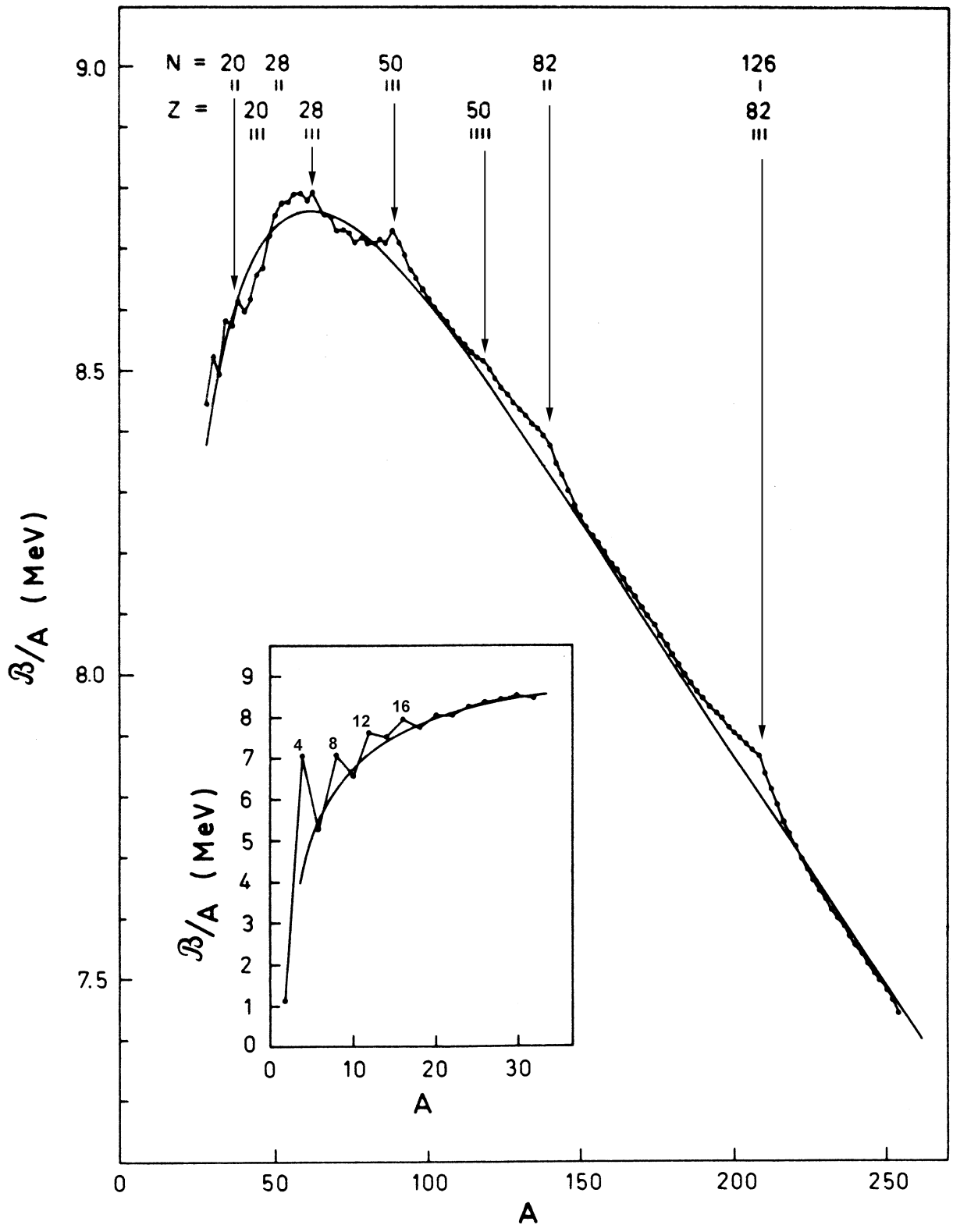

Figure 4. Experimental and theoretical nuclear binding energy per nucleon as a function of mass number showing magic number effects. Note: This is Fig. 2-4 of Ref. 13.

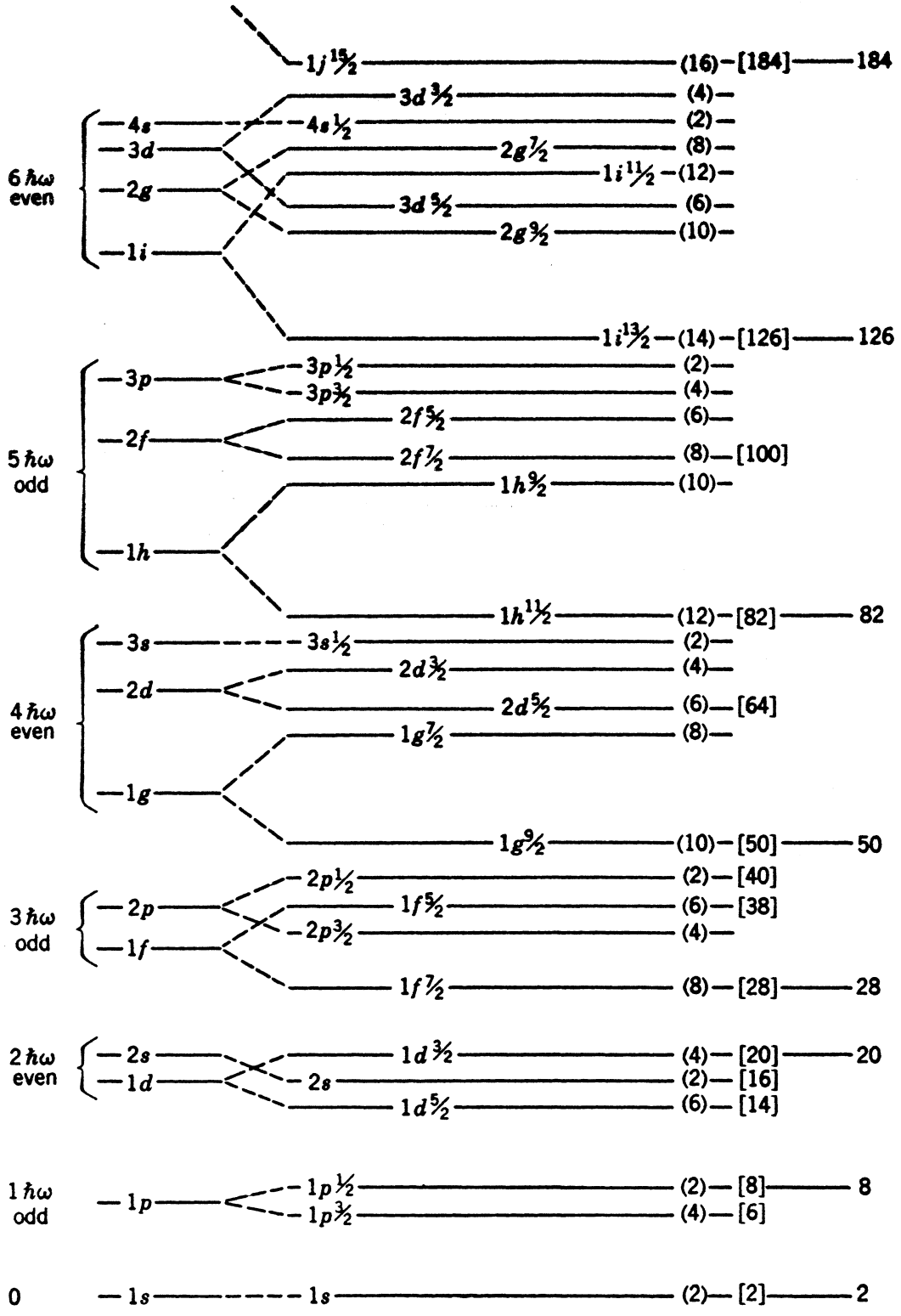

Figure 5. Single-particle energy levels in a nuclear potential well with spin-orbit coupling. Note: This clearly shows energy gaps corresponding to filling with a magic number of particles. This figure is taken from Ref. 14.

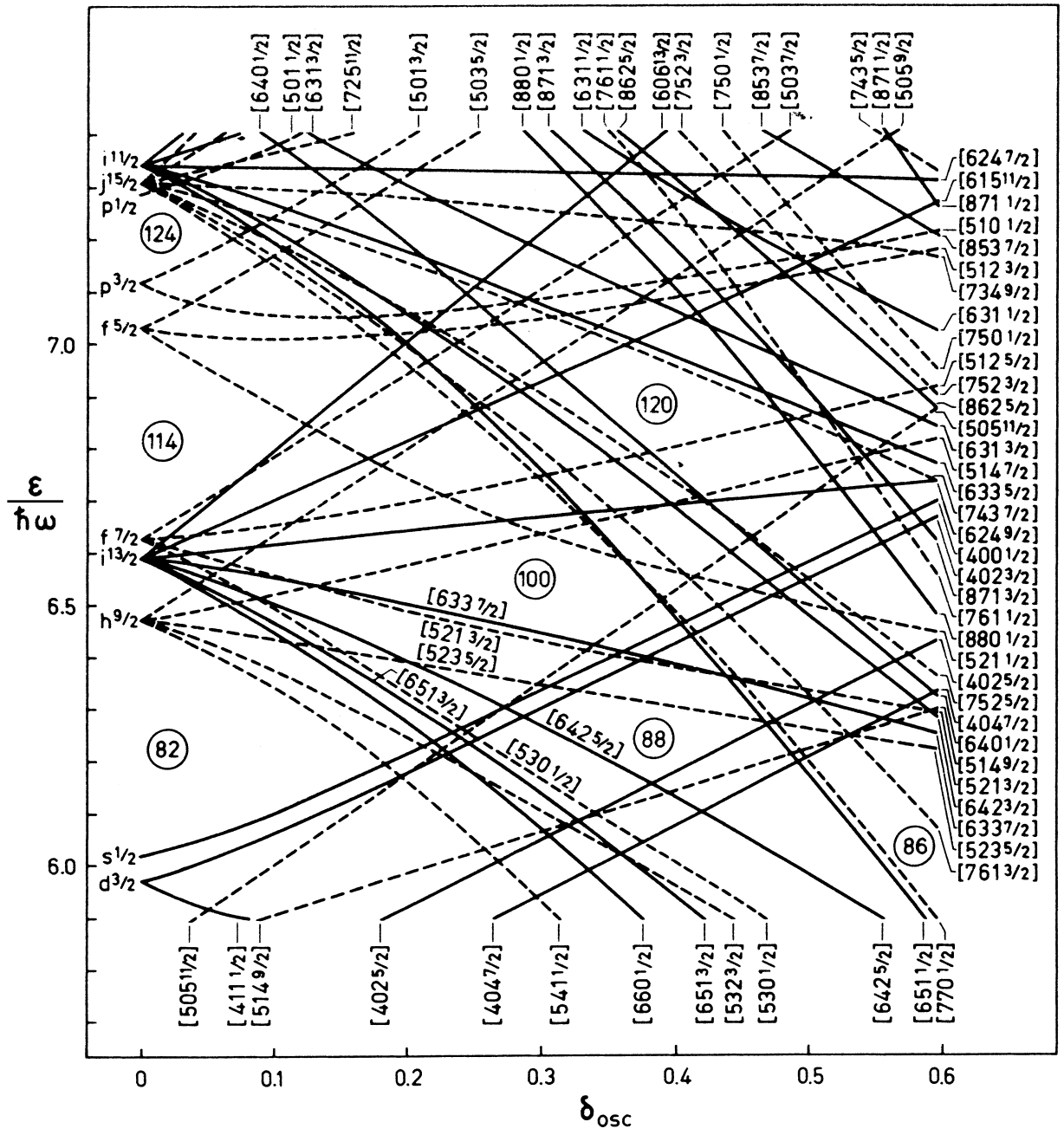

Figure 6. **Nilsson single-particle proton energy levels versus elongation in a spheroidal nuclear potential well of harmonic oscillator form.** Note: Deformation is denoted by δ_{osc} and energy relative to harmonic oscillator frequency by $\varepsilon/\hbar\omega$. Note the "magic number" gaps at certain non-spherical shapes. Each of the levels is labeled with a set of quantum numbers in brackets [ ], the last number being the spin projection on the axis of cylindrical symmetry. This figure is taken from Ref. 15.

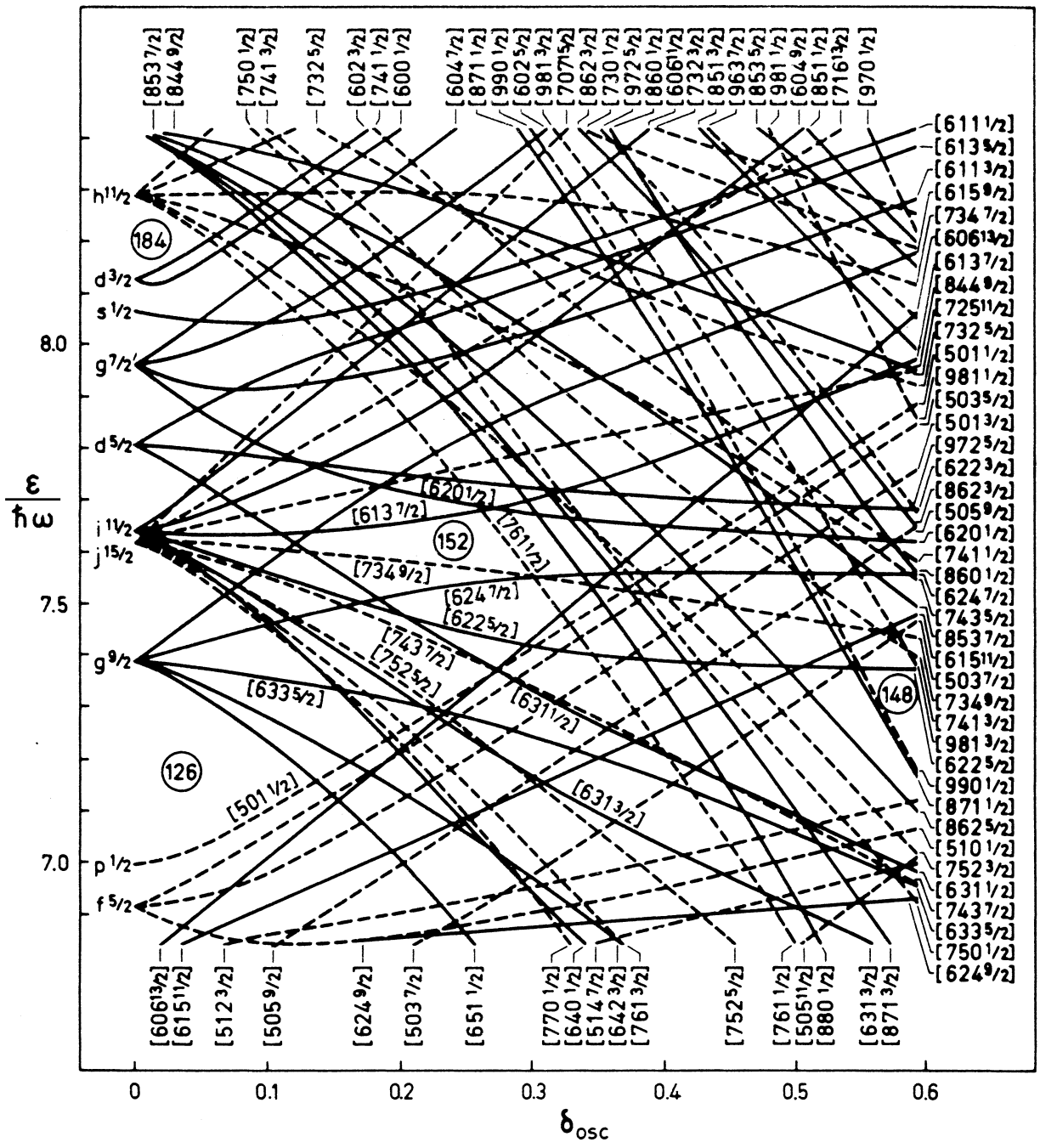

Figure 7. Same as Figure 6, except that these are neutron orbitals. Note: This is taken from Ref. 15.

V. Effect of Nuclear Structure on Fission

Application of these ideas to fission led to Aage Bohr's concept of "saddle-point channels" (also known as transition states).[16] The idea is that part of the nuclear excitation energy is tied up as potential energy of elongation towards fission, leaving at the saddle point only a relatively small amount to divide between kinetic energy of elongation and "internal" excitation of other modes (rotation, vibrations in orthogonal modes, quasi-particle excitation, etc.). These excitations will manifest themselves as quasi-discrete states, and the nucleus will elongate over the barrier in one of these states, which defines a saddle-point channel. For comparatively low excitation energy of the compound nucleus, such as in slow neutron induced fission, only one or a few of these channels will be important.

In 1956, Aage Bohr[16] demonstrated the correctness of the concept by using it to explain the angular distribution of the fission products from photo-fission and fast neutron-induced fission of e-e nuclides.

The implication is that the transition state spectrum is an important consideration in making fission rate estimates. We give here two examples:

a) Specialization energy.

The spin and parity of odd-mass and odd-odd nuclei are significant in spontaneous fission. Because Nilsson levels form such a spreading, inter-weaving pattern with increasing deformation, it is almost certain that quantum numbers of the ground state (at normal deformation) will not be replicated by the lowest transition state, but by a considerably higher state, thus hindering the spontaneous fission decay. See Figure 8.

b) Effect of spin and parity on slow neutron induced fission. Here are two typical cases:

(1) ^{233}U. This has spin and parity $I^{\pi} = 5/2^{+}$, which means that the absorption of a slow neutron gives a compound nucleus ^{234}U with total angular momentum and parity $J^{\pi} = 2^{+}$ (weight 5/12) and 3^{+} (weight 7/12). Both these occur as collective transition states in the energy gap of the transition state spectrum at the saddle point and well below the neutron separation energy.

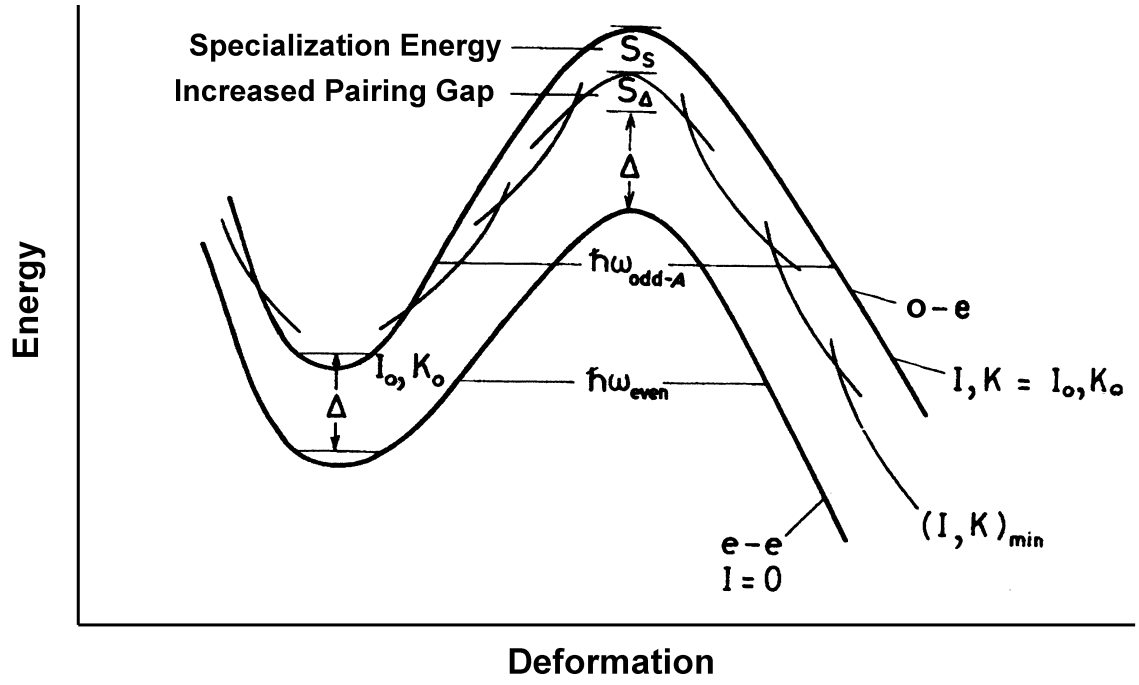

Figure 8. Specialization energy at the fission barrier of an odd-mass nucleus compared to an even mass nucleus. Note: Compared to the barrier of an even nucleus (with spin zero), an odd-A shape isomer sees an increased barrier because (a) the inertia may increase to decrease the $\hbar\omega$ value, (b) the pairing gap Δ may be larger at the barrier by an amount S_Δ, compared to the minimum, and (c) the lowest-lying transition state with $(I,K)^\pi$ value equal to that of the isomeric state may lie an amount S_s above the lowest transition state. This figure is taken from Ref. 17.

(2) ^{237}U. This has $I^\pi = 1/2^+$, leading to a compound nucleus ^{238}U with $J^\pi = 0^+$ (weight 1/4) and 1^+ (weight 3/4). The 0^+ transition state is of course the lowest, so the 0^+ resonances have large fission widths on average. However, the 1^+ transition state is either a 2 quasi-particle state above the energy gap or a high-energy combination of two odd-parity vibrations also above the energy gap. These transition states are higher than the neutron separation energy. Hence, these higher-weighted resonances have much smaller fission widths. The average* fission cross section is much lower for ^{237}U than for ^{233}U (compare Figures 9 and 10 and Figures 39 and 40).

* In this discussion, "average" means the average value over all the resonances within a given energy interval.

(1) ^{233}U – $I^{\pi} = 5/2^{+}$, Compound nucleus — $J^{\pi} = 2^{+}$ (wgt 5/12) and 3^{+} (wgt 7/12)

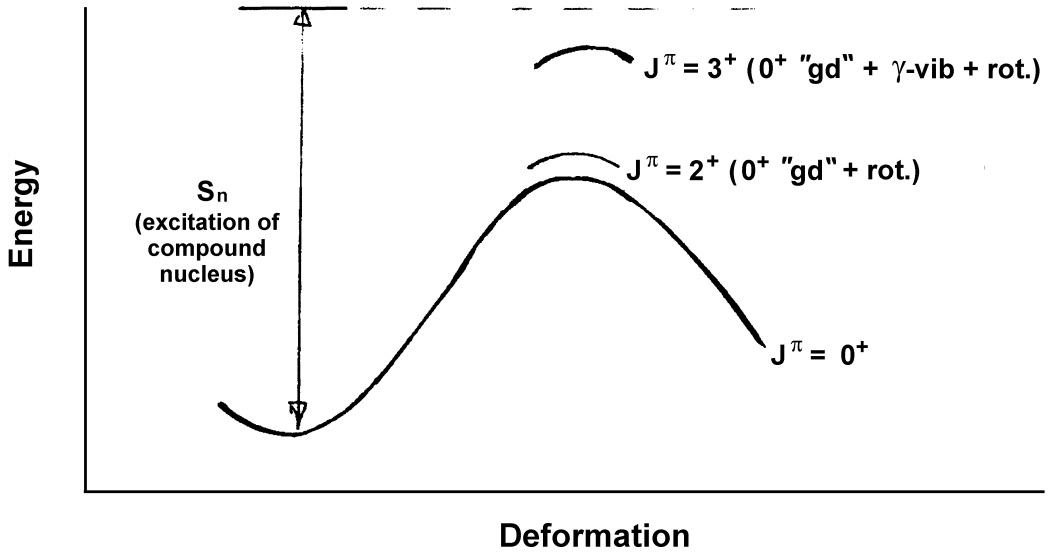

Figure 9. Saddle points for slow neutron induced fission of ^{233}U.

(2) ^{237}U – $I^{\pi} = 1/2^{+}$, Compound nucleus — $J^{\pi} = 0^{+}$ (wgt 1/4) and 1^{+} (wgt 3/4)

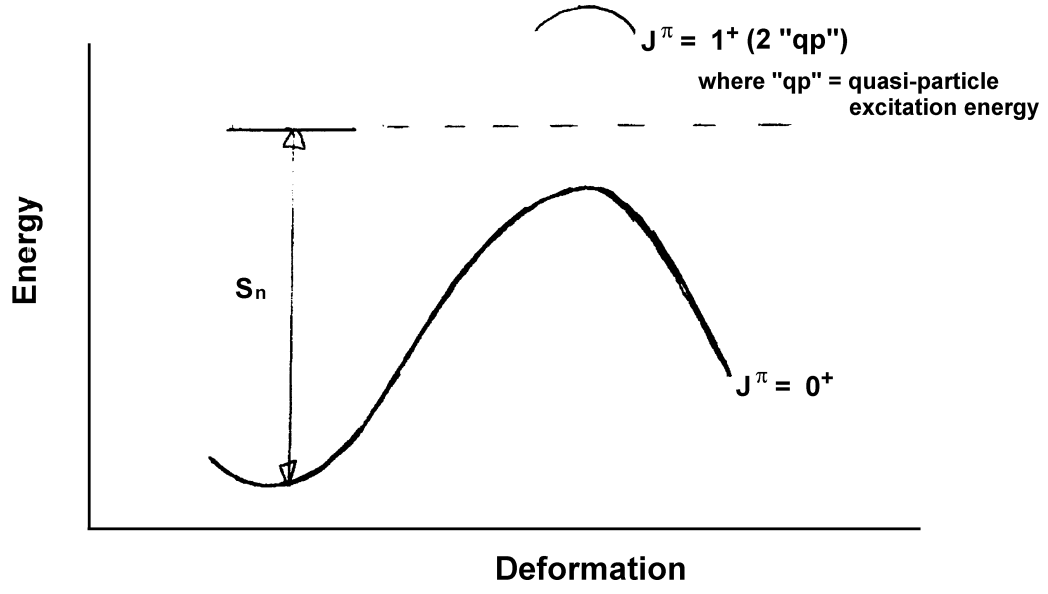

Figure 10. Saddle points for slow neutron induced fission of ^{237}U.

VI. Developments in Fission Physics post-1958

In the discussion above, we already have seen dependence on nuclear properties other than Z^2/A. Now we turn to the developments between Vandenbosch and Seaborg[3] in 1958 and the end of the 1960s.

A) Experimental

1) Spontaneously fissioning isomers (first discovered by Flerov and Polikanov[18])

First let us say something about normal isomers, which are excited states with very long half-lives. These had long been known and were of course well understood. They are generally characterized by some form of electromagnetic decay, normally of very high multipolarity because the relevant spin quantum numbers are very different from those of any lower state. Usually these isomers are less than 1 MeV in excitation energy.

Spontaneously fissioning isomers decay predominantly by fission (vs. electromagnetic decay). Their half-lives are in the range μs to ms, implying that they lie ~ 3 MeV above ground state (cf. ground states ~ 10^{10} yr). Experiments on the rate of formation of spontaneously fissioning isomers as a function of projectile energy confirm this magnitude of excitation energy and also demonstrate that these isomers do not have particularly high spin.

2) Intermediate structure in neutron cross sections

This is best exemplified by the slow neutron cross section of ^{240}Pu. At very low neutron energies the fission cross section is very small. The thermal value is only 56 mb (capture is 290 b) and the fission width of the enormous 1.06 eV resonance is only 6 μeV whereas the capture width is 32 meV. In the upper part of Figure 11, we see the total cross section from about 500 eV to about 3 keV.[19] There are many resonances (spacing about 20 eV) observable over the whole range. By contrast, significant fission cross section only occurs in very narrow, widely spaced groups of these resonances.[20]

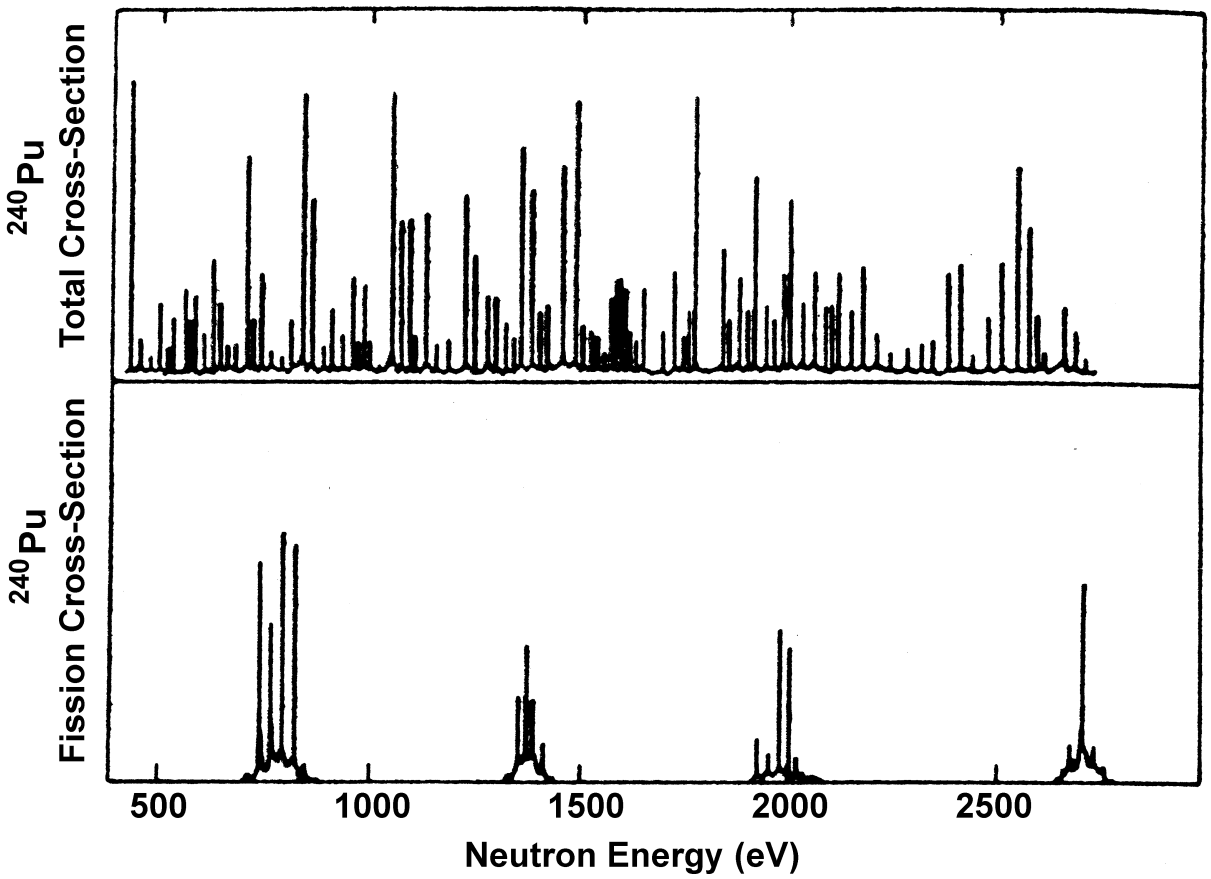

Figure 11. Comparison of ^{240}Pu resonances in the total cross section and the fission cross section. Note: The total cross section is from Ref. 19 and the fission cross section is from Ref. 20.

B) Theoretical (pioneered by Strutinsky[21,22])

Nilsson diagrams had already been used to explain deformed shape stability of far-from-magic-number nuclei. The procedure is to fill levels up to the total number of nucleons, sum energies of the occupied levels, and obtain a plot as a function of deformation. Then, the minimum of the summed energy is the stable deformation.

This runs into difficulties when pushed to much higher deformation.

Strutinsky's idea: Subtract from the above sum a similarly calculated sum over energy levels spread out by a broad averaging function (with width on the order of the energy gap between major shells). The result is the Shell Correction (SC). Then replace the sum over spread levels with the Liquid-Drop Energy (LDE) for that deformation.

Thus, the total energy of the nucleus at a given deformation is the sum of

LDE + SC

A typical result of such a calculation in the actinide region for the shell correction is shown in Figure 12. The abscissa is a measure of elongation. The oscillating structure of the shell correction indicates that magic number effects are not confined to spherical nuclei. This is already shown qualitatively by the energy levels of the deformed harmonic oscillator (Figure 13), which show shell gaps at certain important axis ratios. Superposition of this shell correction on the liquid-drop energy gives (for actinides) the sort of result shown schematically in Figure 14.

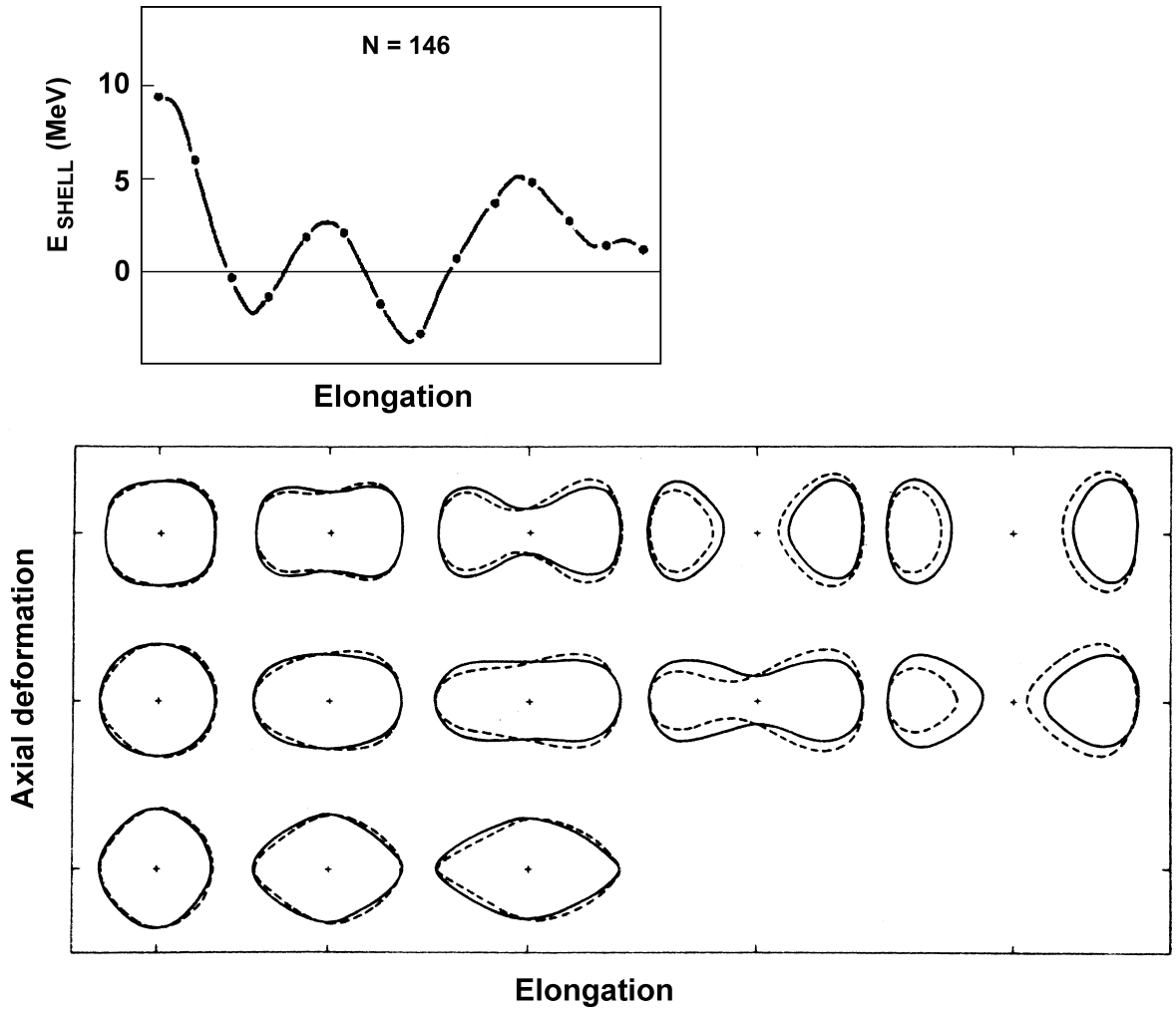

Figure 12. The dependence of the Strutinsky shell correction on elongation of the nucleus and examples of the nuclear shapes considered in these calculations. Note: The shell correction is the upper part which is Fig. 6 of Ref. 23 and the lower part shows examples of the nuclear shapes (from Ref. 24).

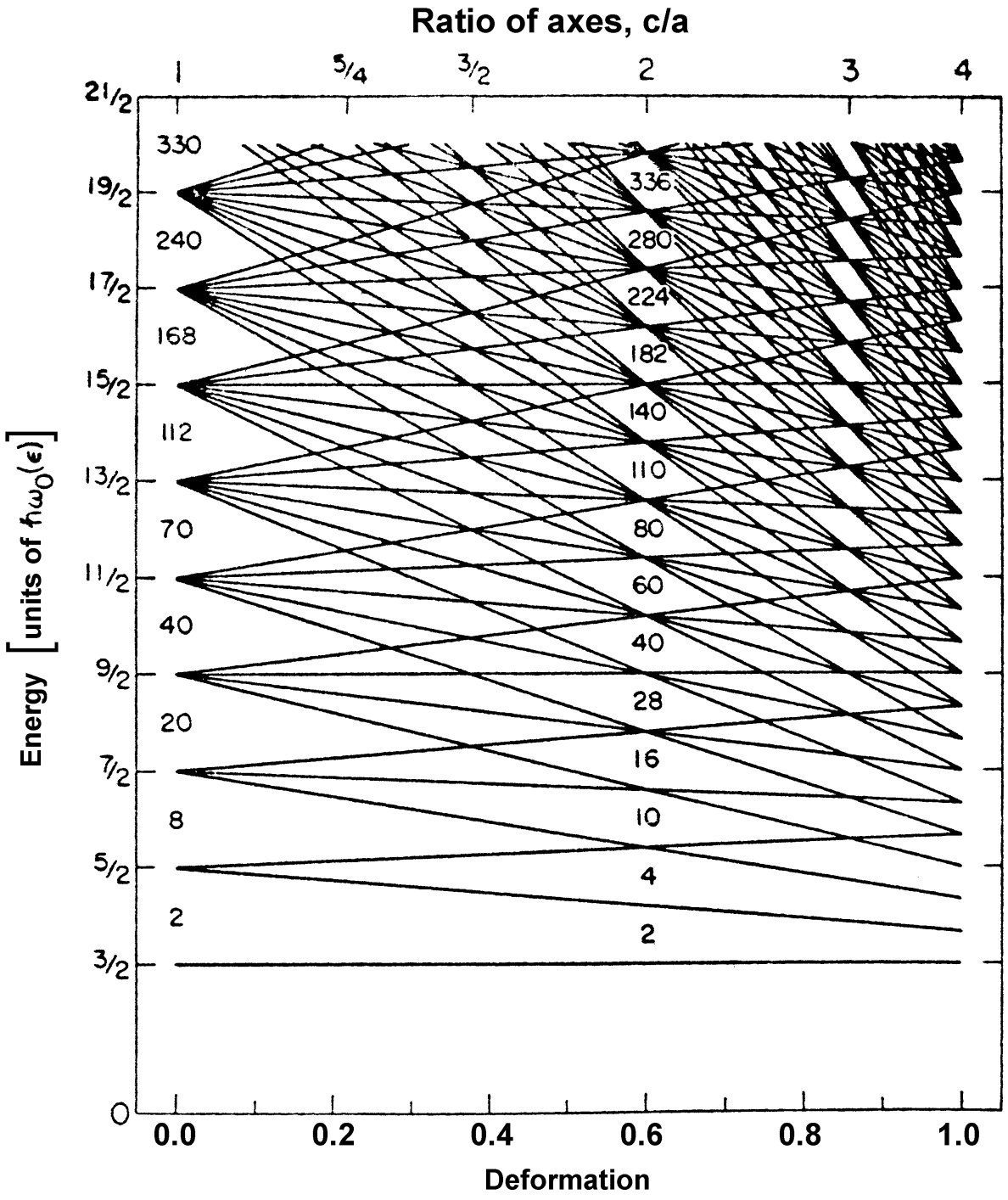

Figure 13. Energy levels of a harmonic oscillator potential for prolate spheroidal deformations. Note: The particle numbers of the closed shells are indicated for a sphere and a spheroid whose major axis is twice its minor axis. This is taken from Ref. 25.

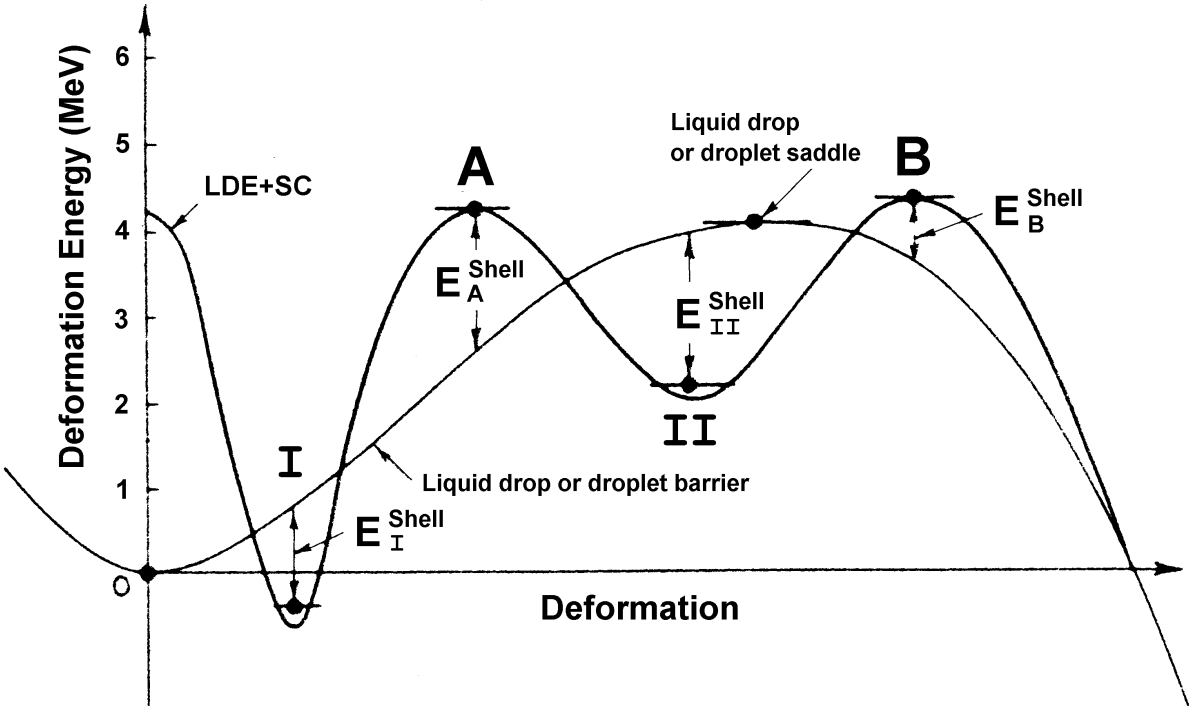

Figure 14. Schematic diagram of the total nuclear deformation energy along the fission path for a nucleus in the actinide region. Note: Shell effects are built on the underlying liquid-drop (or droplet) reference energy. This is from Ref. 17.

VII. The Double-Humped Fission Barrier

The new potential energy curve as a function of deformation immediately affords an explanation of spontaneous fission and intermediate structure (Figure 15).

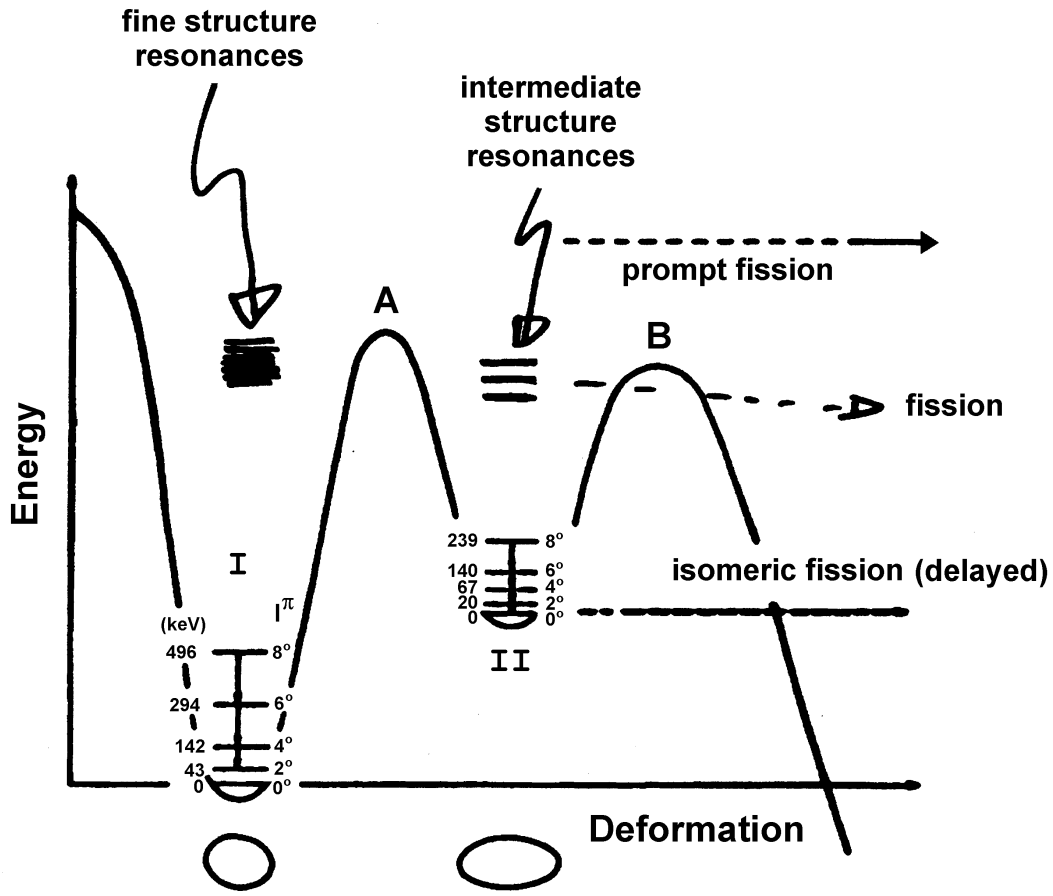

Figure 15. Illustration of the types of levels associated with the double-humped barrier and meta-stable shape of an actinide nucleus. Note: The lowest states shown above the well II use spectroscopic data from Ref. 26. In addition to prompt fission through the intermediate structure (class-II) levels, note the possibility of delayed fission following electromagnetic transitions from the highly excited states down to the shape isomer in the secondary well.

The spontaneously fissioning isomer is the lowest state in the "secondary minimum" of the new potential curve. This secondary well hosts a whole array of increasingly complex states. Just above the neutron separation energy they are the "class-II states" that lie at the center of the intermediate fission resonance groups found in the cross sections of nuclei like ^{240}Pu. These are much more widely spaced than the normal fine-structure resonances, which are "class-I" states in the primary well, because so much of their energy is tied up in the potential difference

between the secondary and primary wells. The class-II states can fission because of their proximity to the outer barrier ("barrier B"). The fine-structure resonances can only fission by coupling through the inner barrier (A) to an energetically close class-II state.

We also see an explanation of the Z^2/A dependence of gross fission barrier height, which has been shown to be much shallower than the LD model would predict (see Figure 24). The shell correction depends qualitatively on long-range changes in both neutron and proton numbers unrelated to Z^2/A, which governs the liquid-drop saddle-point deformation and barrier height. Thus, with increasing Z^2/A, the dwindling liquid-drop barrier height is increasingly reinforced by the first shell-correction maximum that constitutes the inner barrier (A). At low Z^2/A the outer barrier (B) is the higher, and at high Z^2/A the inner barrier (A) is dominant (Figures 16 and 17).

We now discuss the modifications to the fission reaction rate due to the double-humped barrier. The transmission coefficient, T, for a quantal system to cross a barrier is equal to the number of states, N, of intrinsic excitation available to it at the barrier (Bohr and Wheeler[7]) — see Figure 18:

$$T_C = 2\pi\Gamma_C / D = N_C = \int dE' \rho\,(E' - E_F) \qquad (10)$$

Here, Γ_C is the width for crossing the barrier, D is the level spacing (at its equilibrium deformation), and ρ is the 'intrinsic' level density at the barrier deformation as a function of excitation energy above the barrier. The integration is from the barrier energy E_F to the available excitation energy E. This formula was later generalized by Hill and Wheeler[27] to include barrier tunneling:

$$T_C = 2\pi\Gamma_C /D = N_{C,\mathrm{eff}} = \int dE' \rho(E' - E_F)\ \{1 + \exp[-2\pi(E - E') / \hbar\omega_C]\ \}^{-1}\ , \qquad (11)$$

which introduces a tunneling parameter $\hbar\omega_C$ that depends on the barrier penetrability. Following Aage Bohr's introduction of the concept of fission channels (i.e., individual transition states),[16] the integral in this expression can be replaced by a sum over transition states.

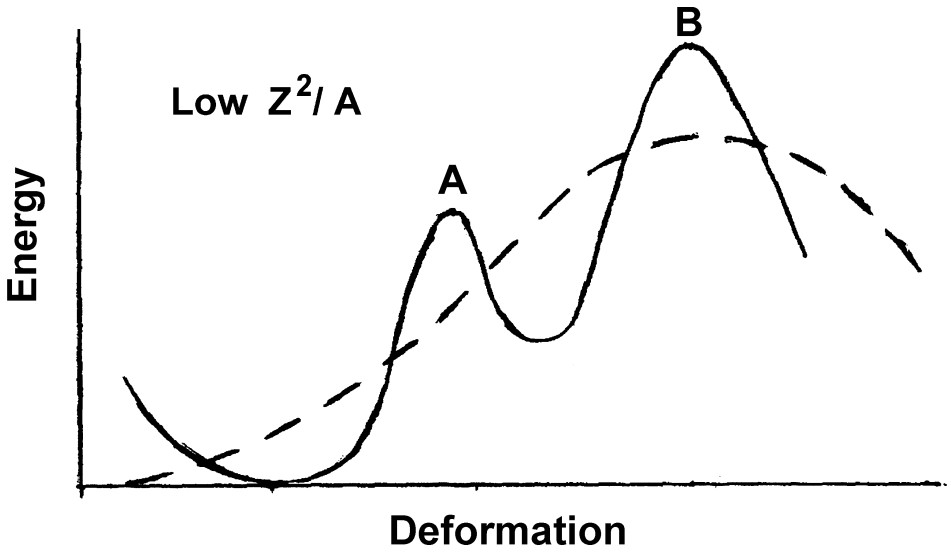

Figure 16. Energy versus deformation for low Z^2/A actinide nuclides.

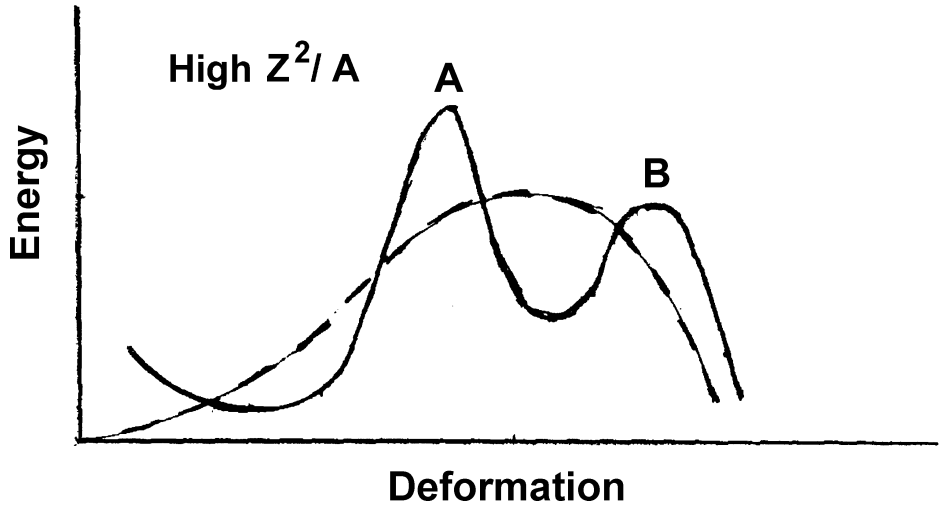

Figure 17. Energy versus deformation for high Z^2/A actinide nuclides. Note: The deformation and energy of the liquid-drop saddle point decreases with increasing Z^2/A and since the shell-correction energy is relatively shape independent, the barrier height of the outer hump is reduced.

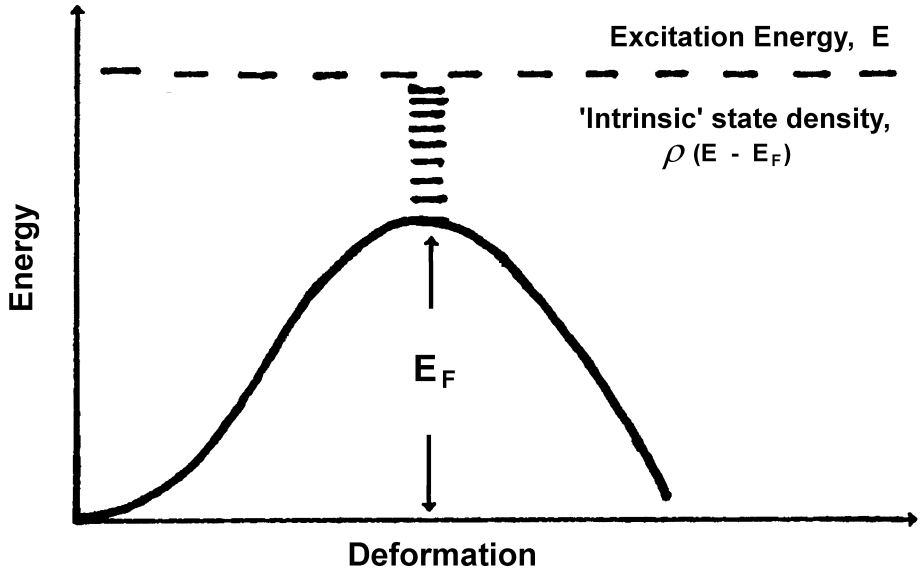

Figure 18. Energetically available 'intrinsic' states at the saddle point used in the Bohr-Wheeler computation of the single barrier transmission coefficient. Note: This is adapted from Fig. 3 of Ref. 7.

When there are two barriers to be traversed, the simple statistical model for the overall transition probability breaks this down into two stages (see Figure 19). First, there is the transmission coefficient, T_A, for crossing the inner barrier A, whereupon the system equilibrates into a super-deformed compound nucleus (highly excited class-II states). This compound nucleus with meta-stable deformation can either cross the inner barrier again or cross the outer barrier B to fission for which the transmission coefficient is T_B. The probability for the latter is $T_B / (T_A + T_B)$. Thus, the overall transmission coefficient for fission is:[28]

$$T_F = T_A T_B / (T_A + T_B) \tag{12}$$

This expression is valid when the available excitation energy is much greater than either or both of the barrier energies (i.e., $N_{A,B,\text{eff}} >> 1$). The transmission coefficient of Eq. 10 is used directly in calculations of average fission cross sections at neutron energies of a few keV and higher:

$$\sigma_f = (\pi / k^2)\, T_n T_F / T = (2\pi^2 / k^2)\, (\Gamma_n / D)\, (\Gamma_F / \Gamma) \tag{13}$$

Here k is the neutron wave number, T is the total transmission coefficient, and Γ is the average total resonance width.

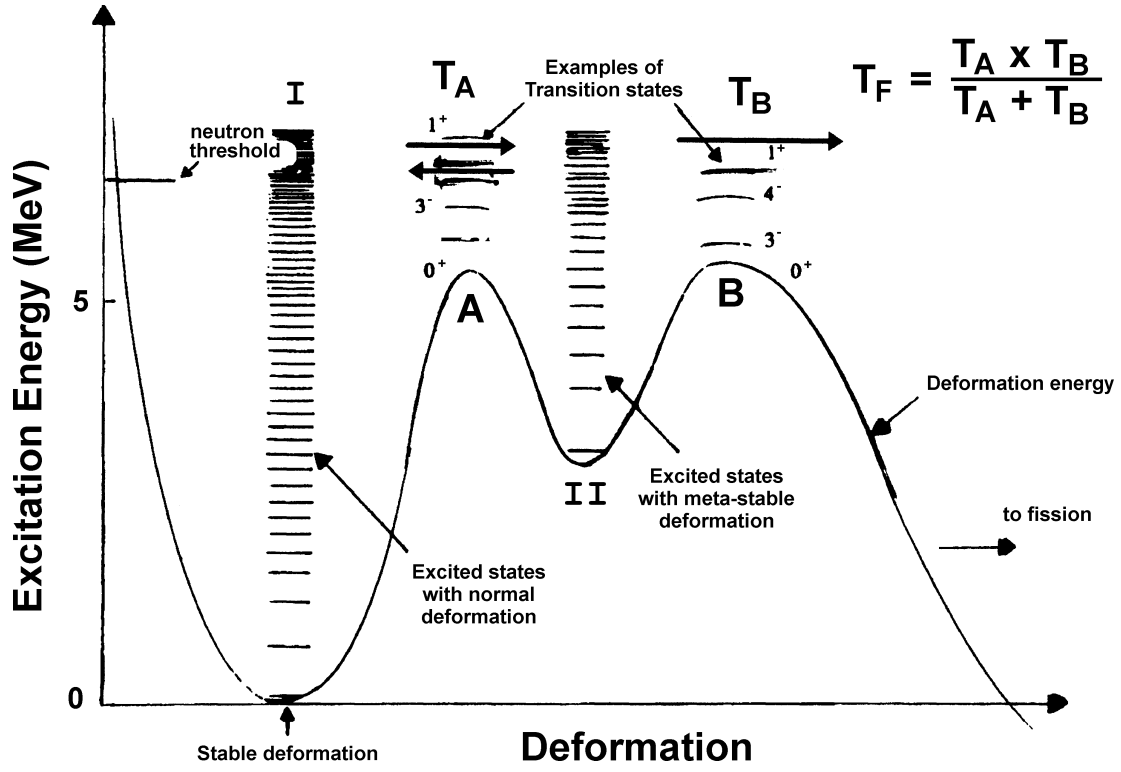

Figure 19. Schematic of the double-humped fission barrier. Note: This illustrates the ways the compound nucleus states can make transitions across the barriers resulting in the overall transition coefficient for fission, T_F .

At energies close to or near the barriers, this statistical approach breaks down. The reason is that the fission strength is clustered into the intermediate resonances. The widths of these are governed by the coupling of class-I (fine structure) states to the class-II states, which is attenuated by tunneling through the inner barrier, and the fission widths of the class-II states, which are attenuated by tunneling through the outer barrier. The clustering of fission strength causes a lower average fission cross section than the value that would be obtained if the fission strength were spread uniformly over the fine-structure resonances. The effect is shown in Figure 20 for a case in which the inner and outer barriers are of equal height. The important curves to compare in this diagram are the curve marked SP, which is the fission probability deduced from the statistical model of Eq. 12, and the curve marked IP, which takes into account the intermediate structure. In these contexts the letter P indicates prompt fission, meaning that the class-II state decays directly by fission. The other possibility is that the class-II state decays by radiation to lower states in the secondary well. After cascading to the shape isomer, delayed fission from this state can occur. This is denoted by D in Figure 20 and is calculated by assuming that the branching ratio for fission from the shape isomer is unity. The other

possibility is that it decays radiatively to lower states in the primary well, cascading eventually to the ground state.

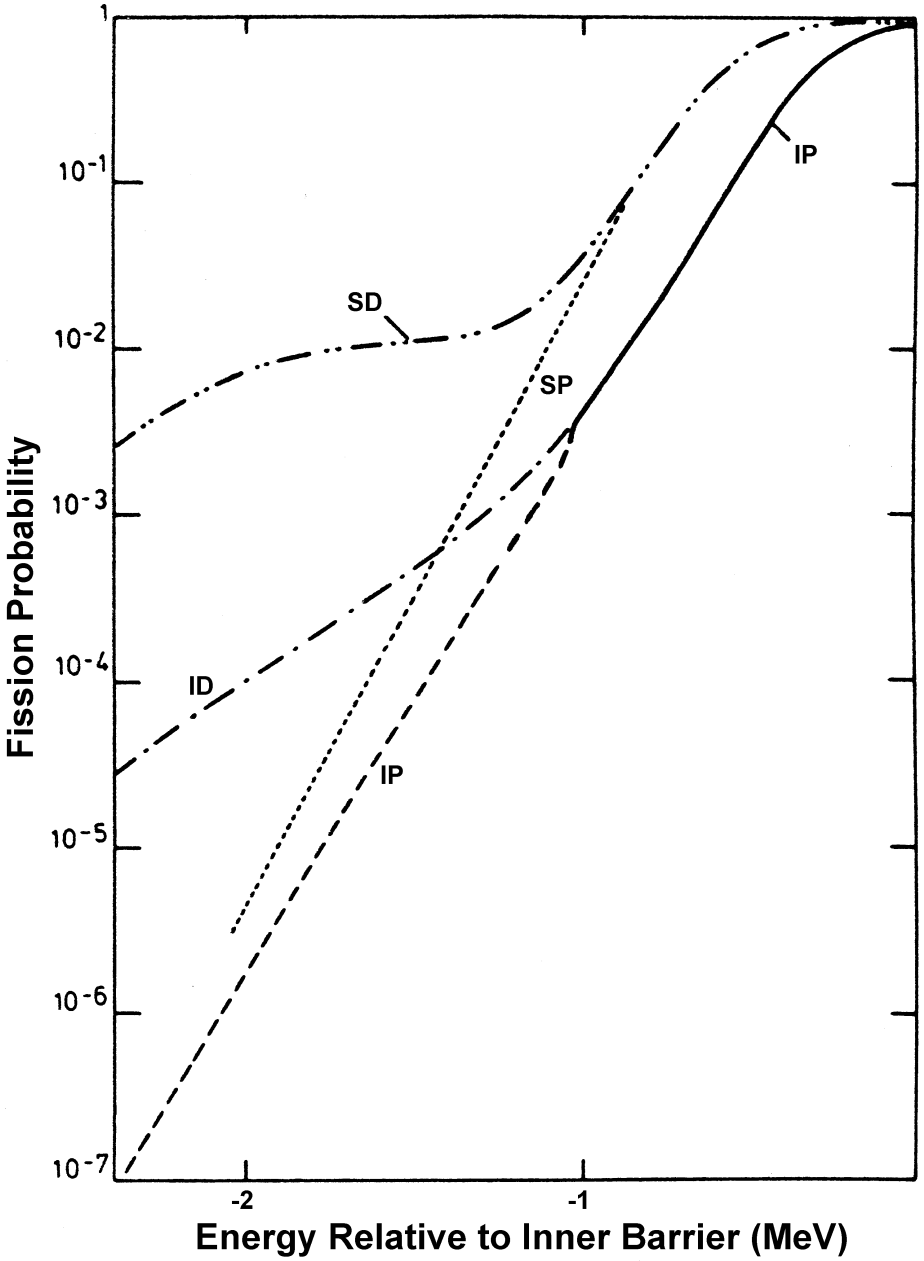

Figure 20. Probability of fission decay of an even compound nucleus with equal barrier heights lying below the neutron separation energy. Note: This is adapted from Ref. 17. The fission probabilities are calculated under various assumptions. The curve marked SP is the simple formula based on the assumption that the intermediate structure resonances are completely washed out. The curve IP takes into account the intermediate structure in the fission cross section in a simple way.

VIII. Other Data Available on Fission Barriers of Actinide Nuclides

Apart from (n,f) data there are data from fission of nuclides that are reached via particle transfer reactions, such as (^{3}He,d,f),* (d,p,f), (t,p,f), etc. These reactions and the photo-fission reaction can give information on fission probability at excitation energies well below the neutron separation energy and thus give valuable information on fission barrier parameters of fissile nuclides as well as on nuclides for which samples for (n,f) measurements are not readily available. Some examples of this kind of data are shown in Figure 21.

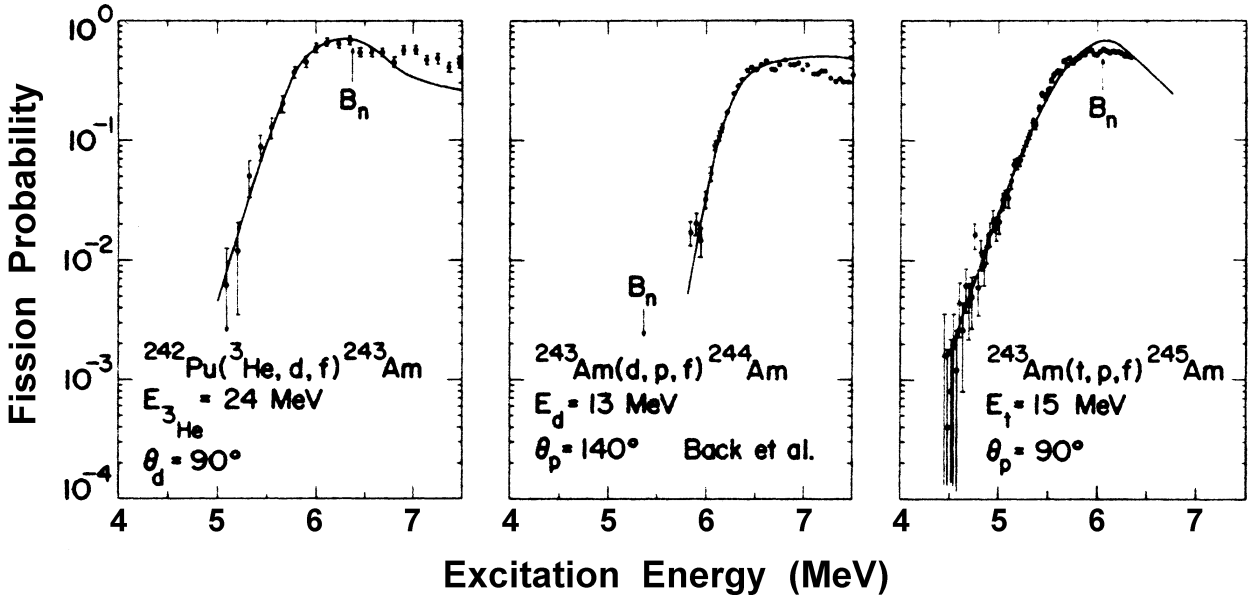

Figure 21. Fission probabilities as a function of excitation energy in the compound nucleus. Note: The neutron separation energy is denoted B_n. These probabilities were measured by particle transfer reactions followed by fission and competing processes. Taken from Ref. 29.

It is possible to analyze data of all these kinds to obtain barrier parameters for a wide range of nuclides. Three different ways of plotting the results are shown in Figures 22 to 24. The outer barrier height is shown as a function of neutron number in Figure 22. Although dependent on neutron number for a given proton number, the main characteristic is a strong downward dependence on proton number. In Figure 23 the dependence of the inner barrier height on Z^2/A is shown. Here, neutron effects are apparent but there is no strong dependence on proton number. In Figure 24 the inner barrier is plotted as a function of Z^2/A relative to the energy of a liquid-drop sphere. It can be seen that the difference between the inner barrier

* In this nomenclature, a helium-3 nucleus is absorbed, a deuterium nucleus is emitted, and the resulting nuclide fissions. For the other reactions, *p* means a proton and *t* means a tritium nucleus.

and the ground state energy (the lower set of points) falls relatively gently, while the liquid-drop saddle-point energy falls rapidly. It is also clear that the inner barrier, which is normally the dominant barrier, falls much less rapidly with increasing neutron number than does the neutron separation energy. This leads to a breakdown of the even-odd parameter as a reliable indicator of fissionability.

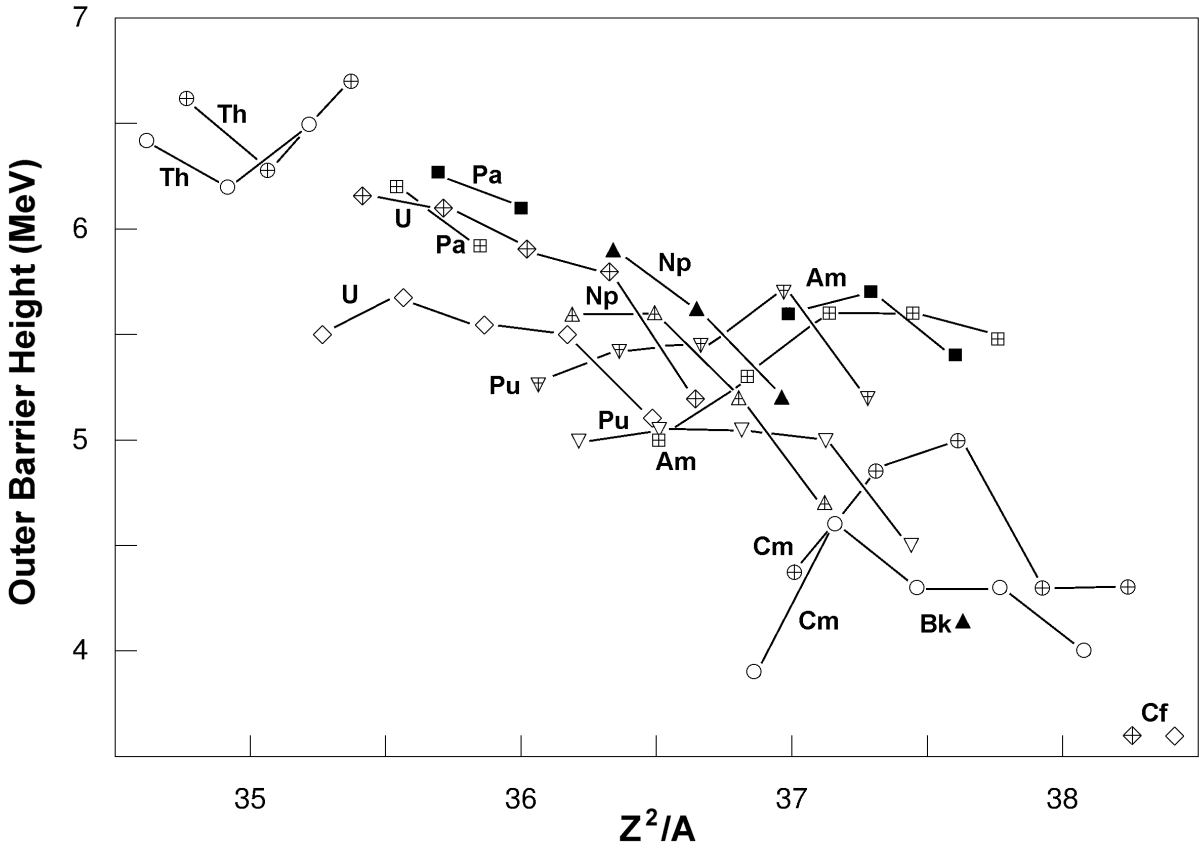

Figure 22. Outer barrier heights as a function of Z^2/A and deduced from a variety of fission-inducing reactions. Note: This is adapted from Ref. 17. Open symbols denote e-e nuclides, crossed symbols denote e-o or o-e, and black symbols denote o-o.

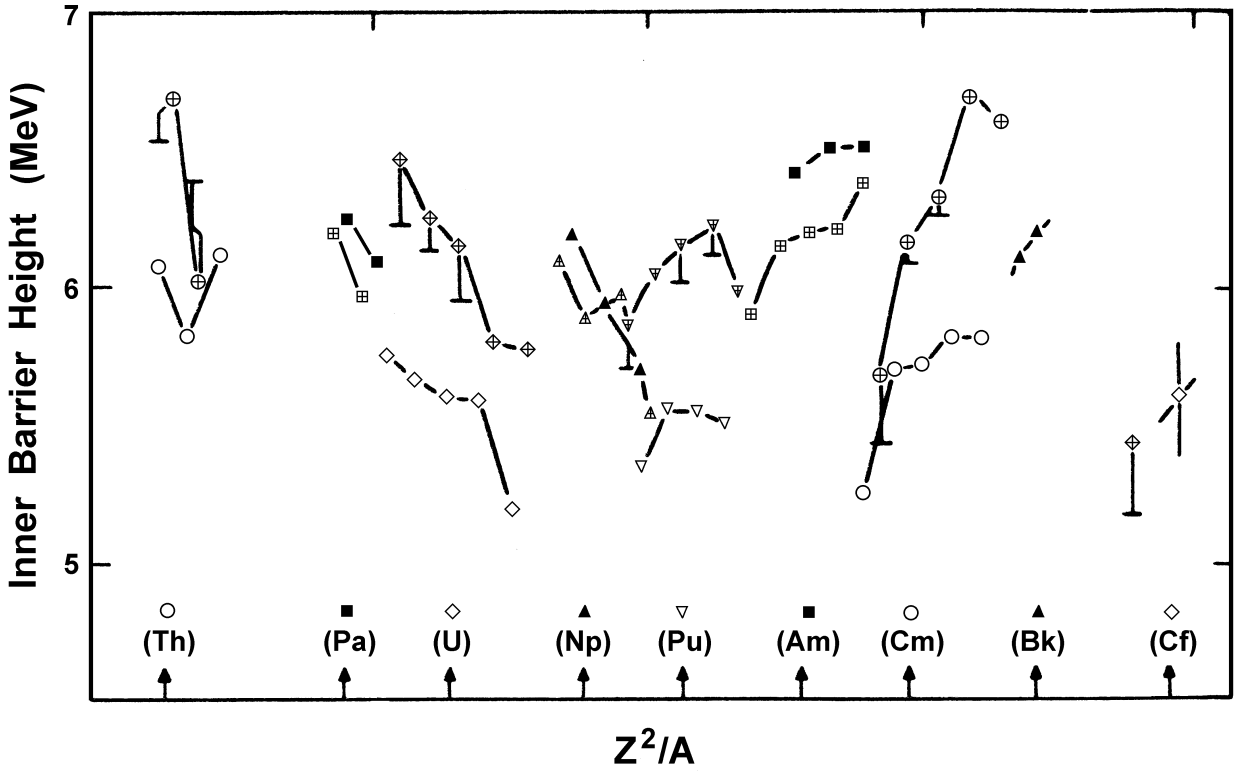

Figure 23. Inner barrier heights as a function of Z^2/A. Note: This is taken from Ref. 17. Open symbols denote e-e nuclides, crossed symbols denote e-o or o-e, and black symbols denote o-o.

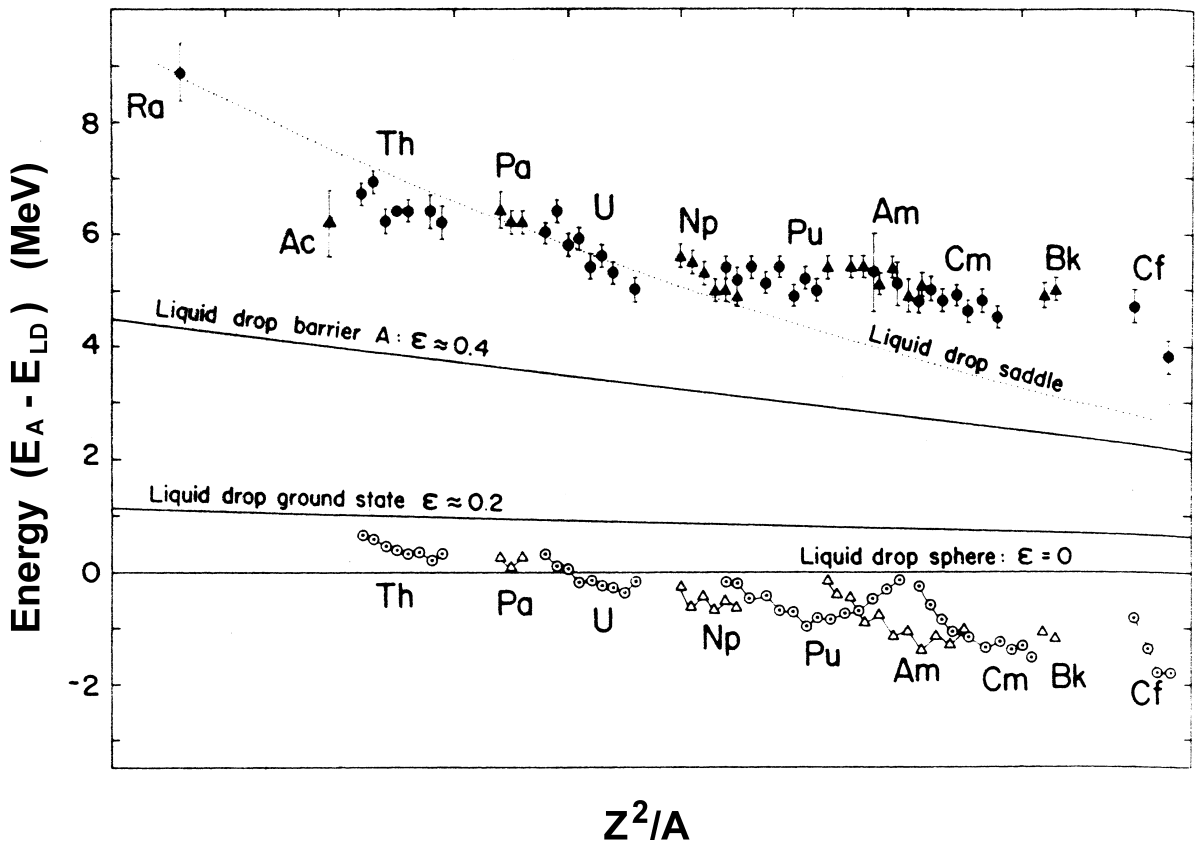

Figure 24. Experimental binding energies for the ground states and for the inner barrier plotted relative to the spherical liquid-drop energy (1967) as a function of Z^2/A. Note: This is taken from Ref. 17. The ground state is denoted by an open symbol and the inner barrier is denoted by a filled symbol. Even-Z elements are represented by circles, odd-Z elements by triangles. Also shown are the liquid-drop deformation energies for two fixed deformations corresponding to the ground-state shapes and inner barrier shapes, and the energy of the (variable) saddle-point shape.

IX. Multidimensional Aspects of the Fission Barrier

So far we have been discussing the fission barrier as if there were only one significant parameter, the elongation variable. But there are other very significant parameters in the Potential Energy vs. deformation landscape.

Examples:

1. The mass asymmetry variable.

This is in fact very important for the main actinides in reducing the height of the outer barrier (by a few MeV). See Figures 25 and 26. Figure 25 shows the deformation energy (liquid-drop and with shell correction) for elongation constrained to mass symmetry, while Figure 26 shows the deformation energy at the outer saddle point as a function of mass asymmetry. The reduction in energy at smaller deformations is insignificant.

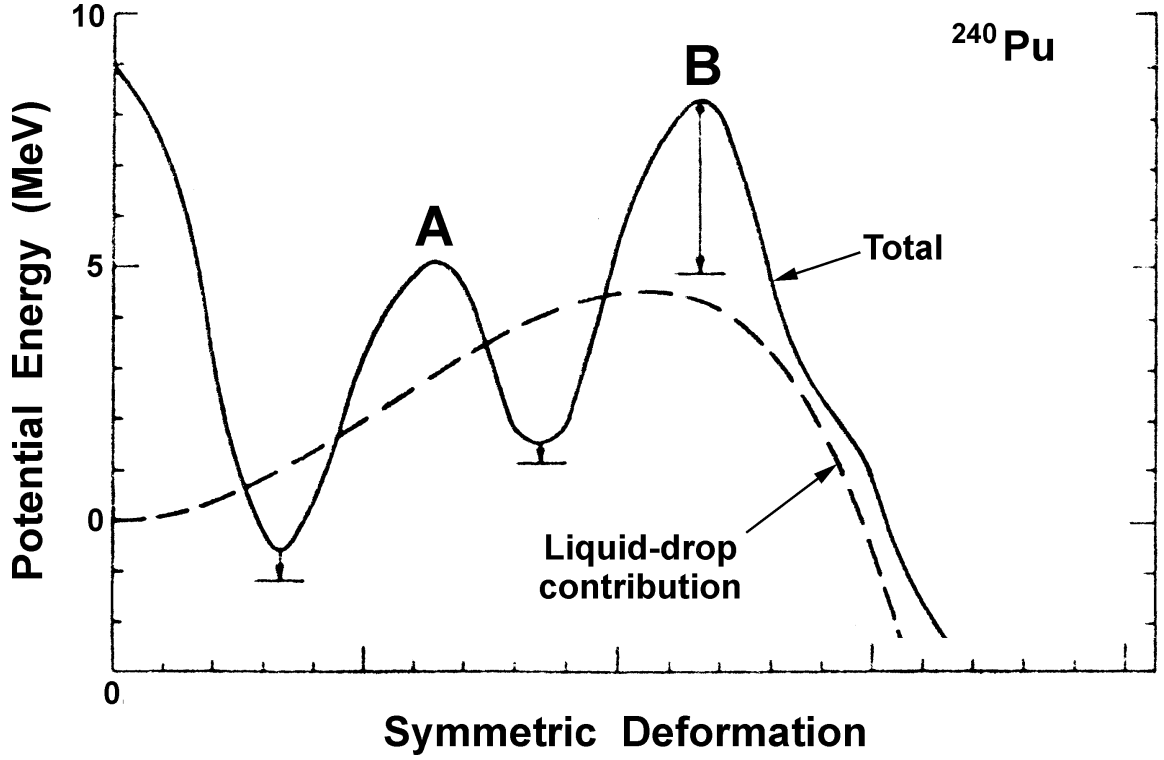

Figure 25. The nuclear energy calculated as a function of prolate deformation for axial and reflection symmetric shapes for ^{240}Pu using Strutinsky's prescription. Note: This is adapted from Fig. 9 of Ref. 17. Arrows on the outer barrier *B* shows lowering of the barrier calculated from reflection asymmetric deformations.

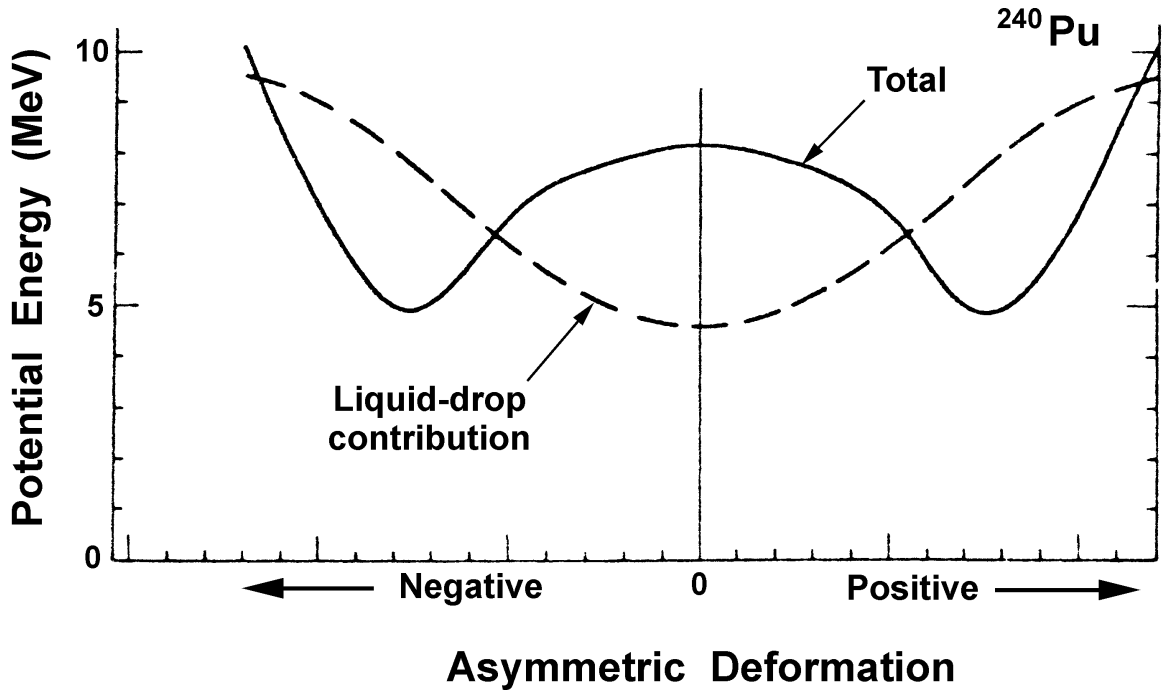

Figure 26. The energy as a function of mass asymmetry for a fixed deformation at the outer barrier. Note: This is adapted from Fig. 9 of Ref. 17. The dashed line indicates the liquid-drop deformation energy.

The mass asymmetry effect is even more significant for the thorium nuclides because it creates a shallow tertiary well within the outer barrier (Figure 27).[30] This causes a second class of intermediate structure. These tertiary intermediate states are often very simple in nature (e.g., a rotational band built on a single quasi-particle mode). The nature of the coupling and resulting fission cross section is shown schematically in Figures 28 to 30. The fission cross section of ^{230}Th from 0.6 to 1.5 MeV is shown in Figure 31. The resonance-like structure near 700 keV is not, of course, a fine-structure resonance like those found in slow neutron cross sections. A higher resolution view of it is shown in Figure 32. The substructures apparent within it are individual tertiary-well states, each with separate spin and parity quantum numbers, as revealed by the fission product angular distribution. The intermediate (class-II) and fine (class-I) structure shown in the schematic of Figure 29 are on too small an energy scale to be revealed by the resolution in Figure 31. In fact the tertiary-well states form two very close vibration-rotation bands, the vibrations being the zero-point motion and first phonon of a tunneling mode through the potential hill separating the two mass-asymmetric valleys shown in Figure 26.

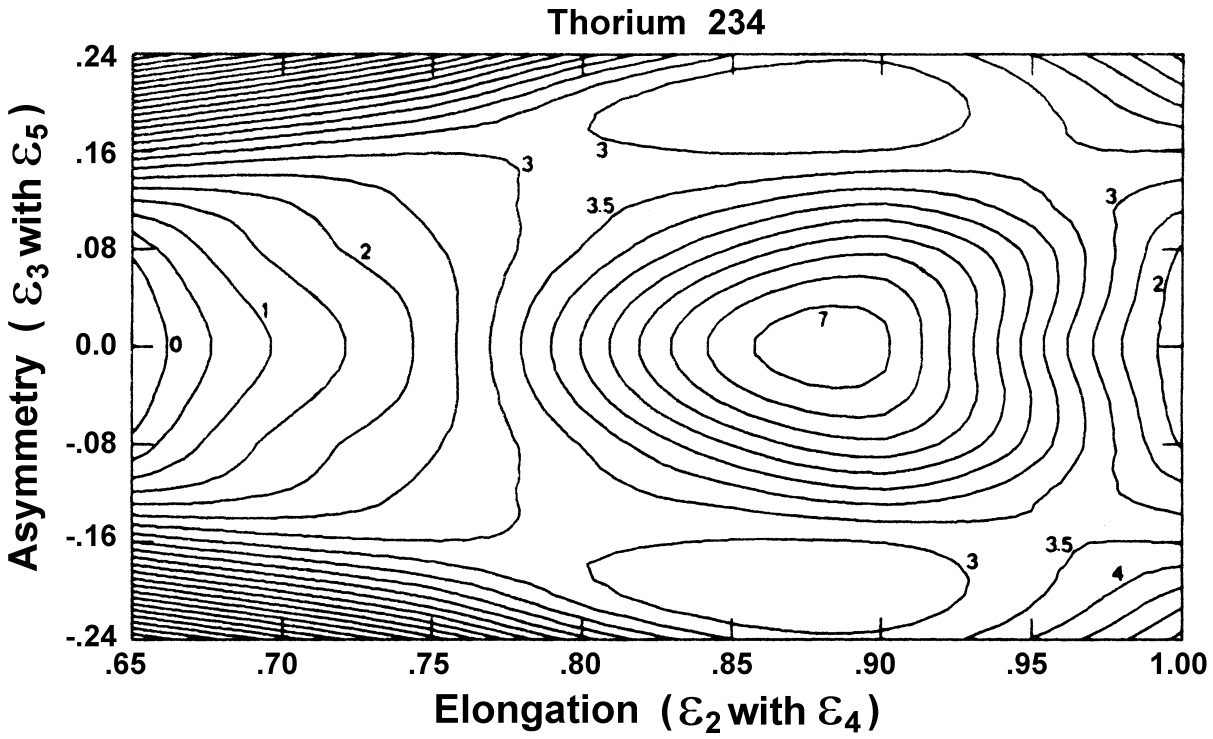

Figure 27. The mass-asymmetric outer fission barrier for ^{234}Th calculated at zero angular momentum in a deformed oscillator model. Note: This is taken from Ref. 30. The potential energy surface is shown as a function of elongation and asymmetry.

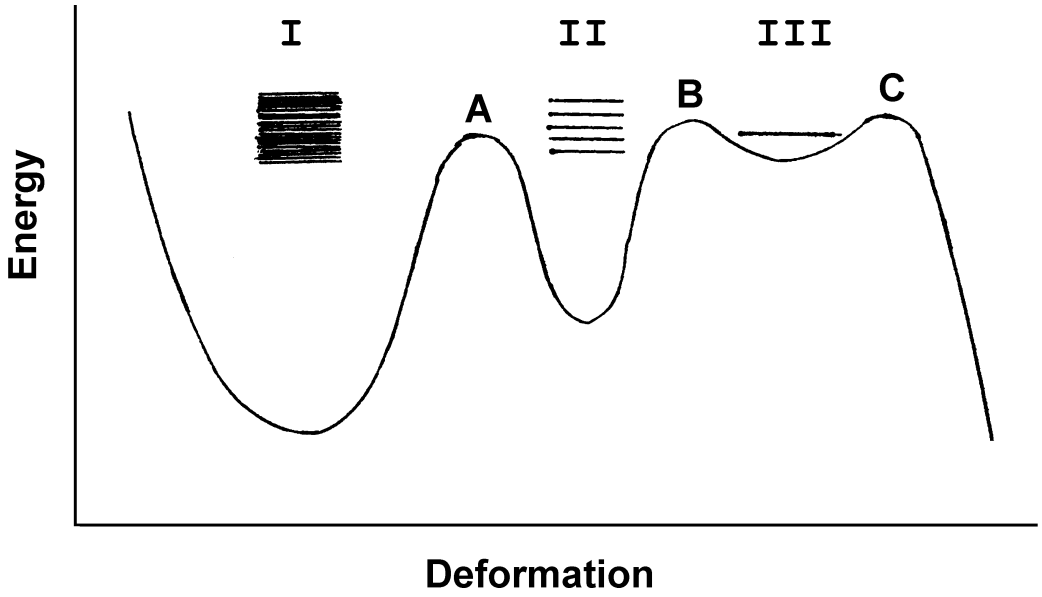

Figure 28. Schematic illustration of the relative density of states in the primary, secondary, and tertiary wells of a triple-humped barrier.

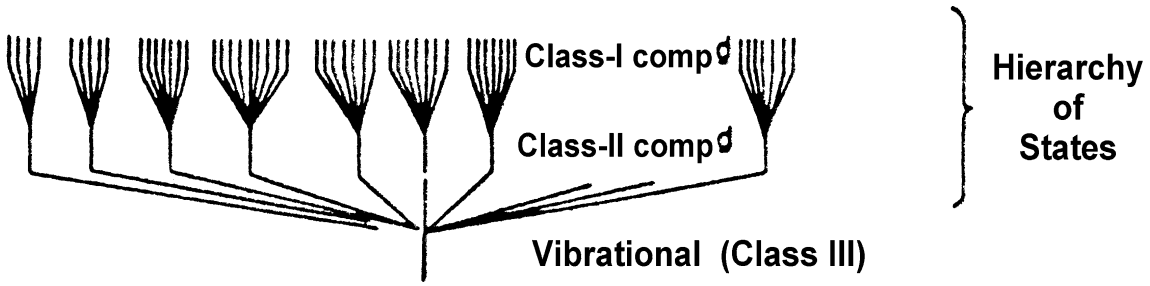

Figure 29. Schematic illustration of the substructure in the fine (Class I), intermediate (Class II), and tertiary (Class III) wells of a triple-humped barrier. Note: This is adapted from Fig. 25 of Ref. 31.

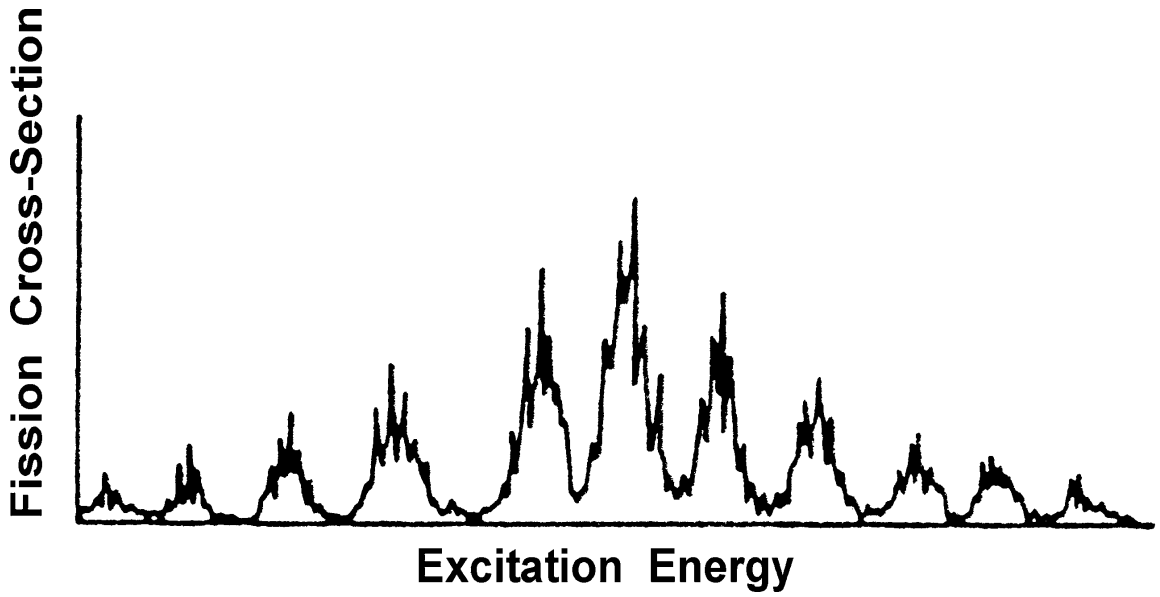

Figure 30. Schematic illustration of the fission cross section of Th nuclides. Note: This is adapted from Fig. 25 of Ref. 31.

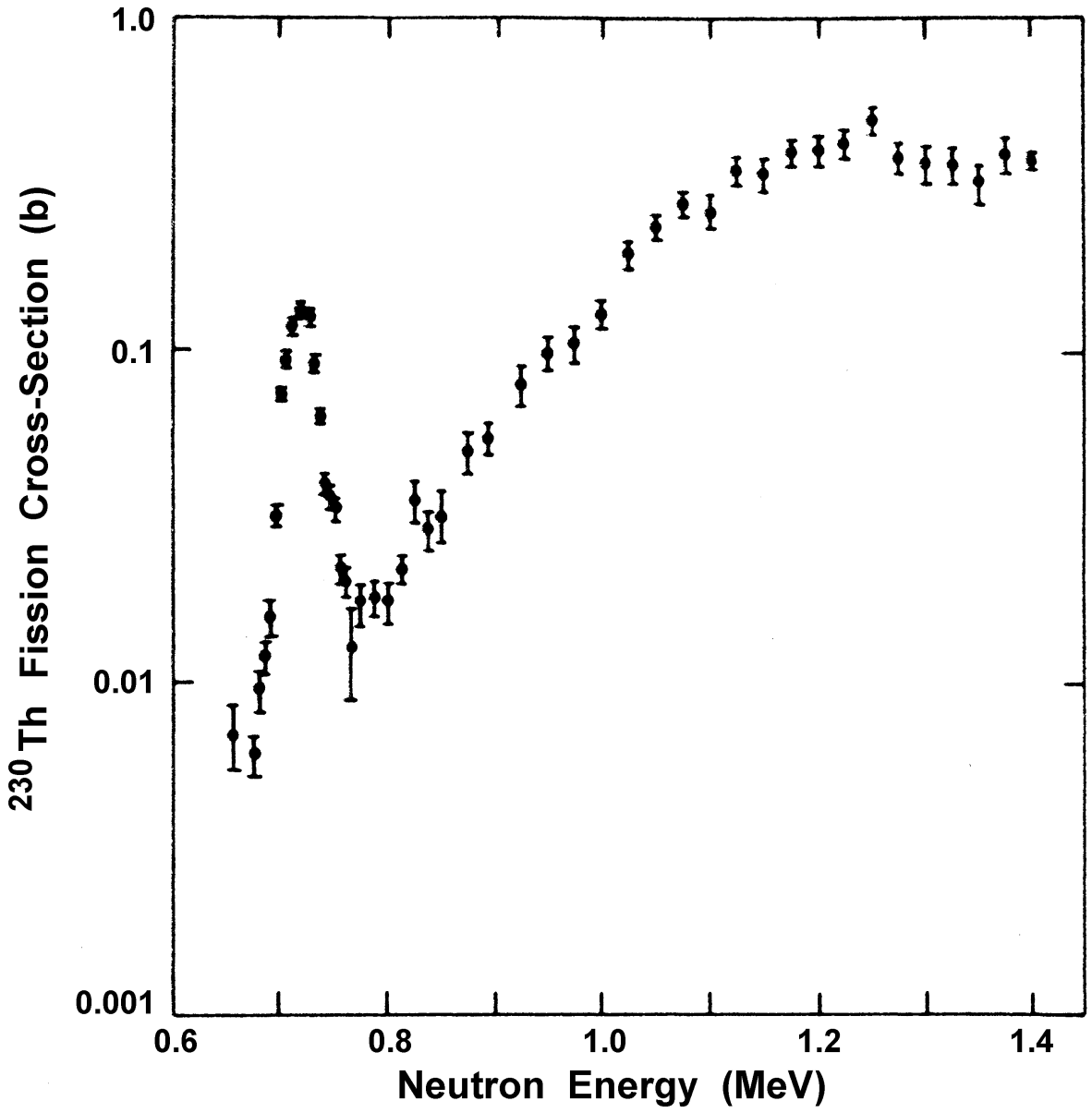

Figure 31. Fast neutron-induced fission cross section of ^{230}Th versus energy of the incoming neutron. Note: The scale of the "resonance" is in tens of keV rather than the tens of meV associated with fine-structure resonances. This is taken from Ref. 32.

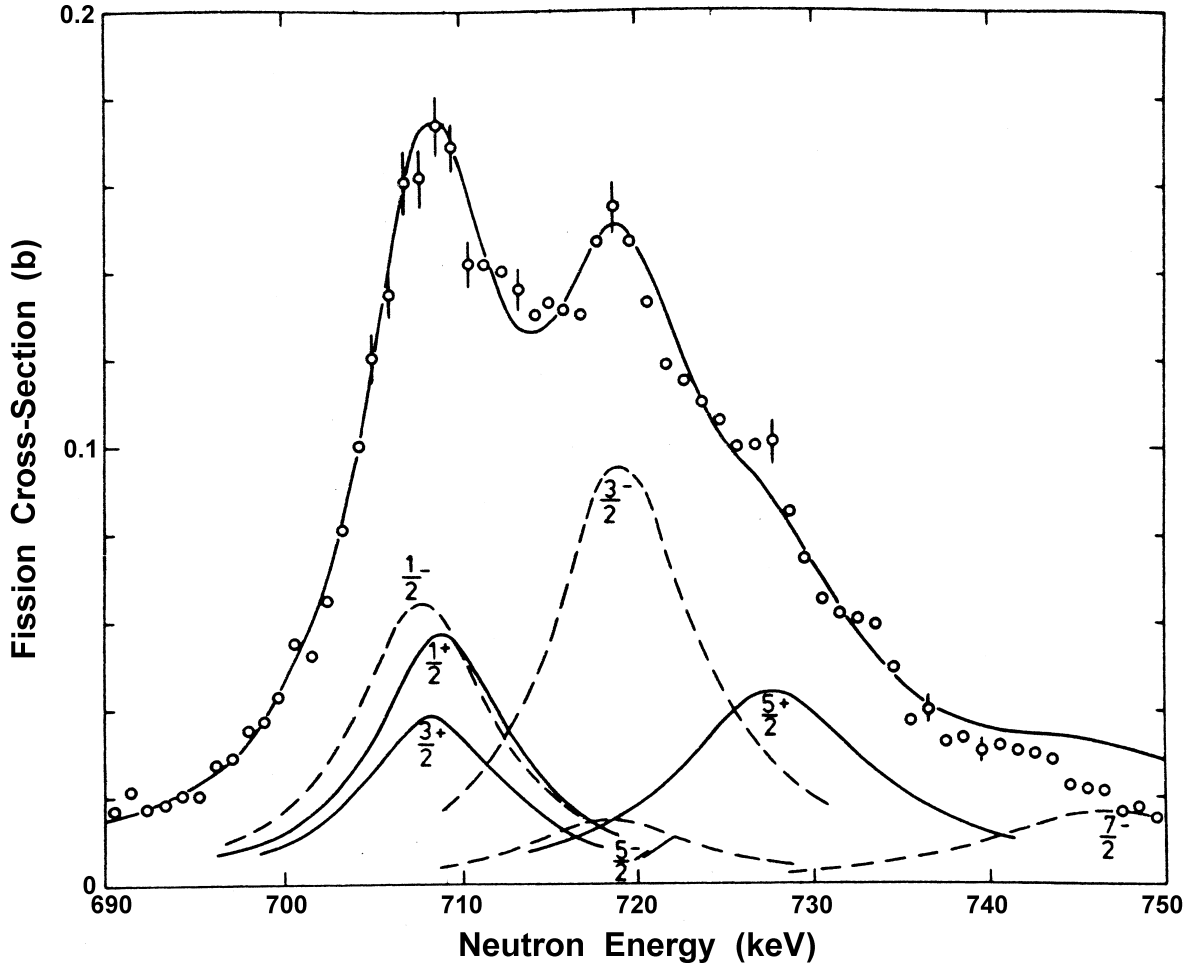

Figure 32. High-energy resolution data for the "resonance" shown in Figure 31. Note: This shows how the structure can be explained (with the aid of fission product angular distribution data not shown here) into rotational bands, one of which is based on a low energy, opposite parity, mass-asymmetry tunneling vibration between the two shallow tertiary wells of Figure 27. This is based on Fig. 14 of Ref. 33.

2. Gamma-asymmetry in the inner barrier

Gamma asymmetry is deformation away from axial symmetry of the deformed nucleus. According to theory, it appears to become pronounced in the uranium isotopes and above. The difference in energy between a strictly axial elongation and one in which axial asymmetry is an allowed degree of freedom is shown for the inner barrier in Figure 33. Apart from lowering the inner barrier by a significant amount, it has the effect of bringing down a denser and more complicated structure of rotational bands. This increases fission width and fission cross section above the barrier. Axial symmetry is energetically preferred for the outer barrier.

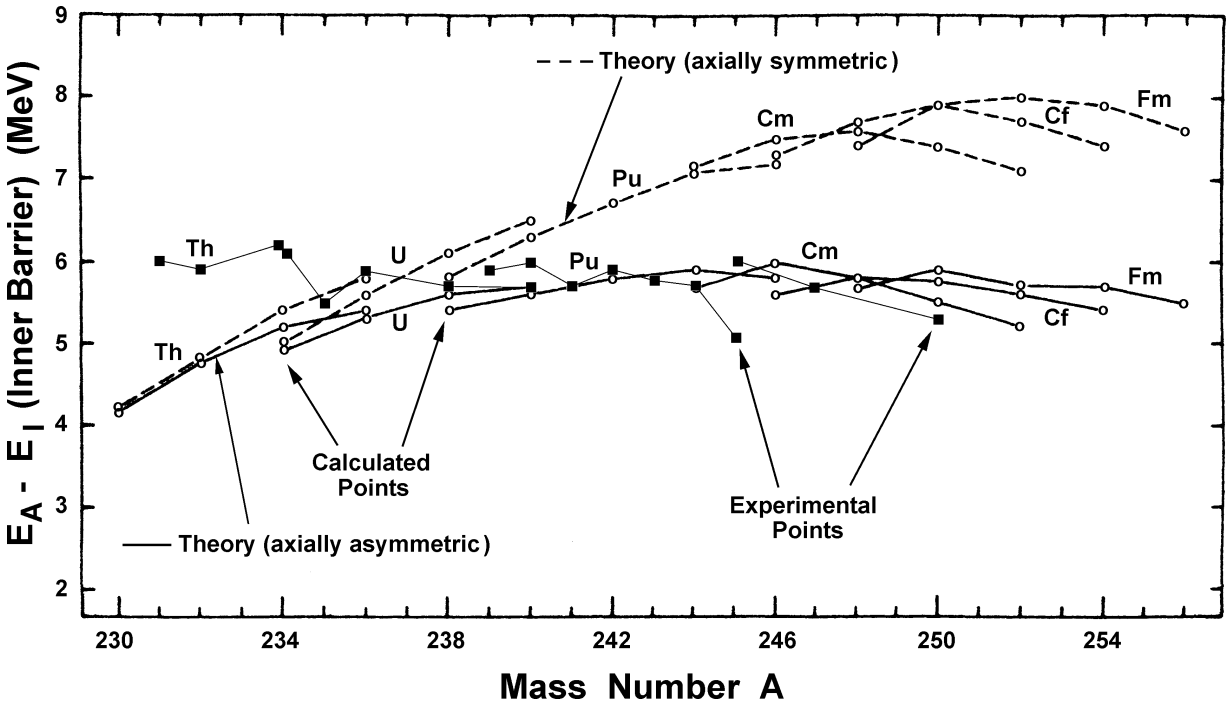

Figure 33. Inner barrier height calculated with and without axial asymmetry, compared to the experimental inner barrier heights. Note: This is taken from Fig. 6 of Ref. 34. The filled squares are experimental values for the gross barrier height, which is usually the inner barrier for U and higher *Z* nuclides.

3. Potential energy surfaces near proton number 100 and neutron number 164

Because of the proximity of particularly strong magic numbers at large deformations, the potential energy surfaces of fissioning nuclei approaching the mass number 264 can be especially complex. The significance of $Z = 100$ and $N = 164$ is that these together form two doubly magic ^{132}Sn nuclei, which are spherical nuclei with very strong binding. Hence there is a very strong tendency for the parent nucleus, as it becomes sufficiently elongated, to divide nearly symmetrically into spherical fragments. In this case, because there is so little energy of the original nucleus tied up in deformation of the fragments, the fission products have high kinetic energy. However, at a much earlier stage of elongation, it is still possible for the nucleus to follow a more traditional path akin to that of the lower actinides. In this case the resulting fragments show asymmetric division, are highly deformed and have much lower kinetic energy. Calculations of the potential energy surface (Ref. 35) show that the situation is even more complicated than this.

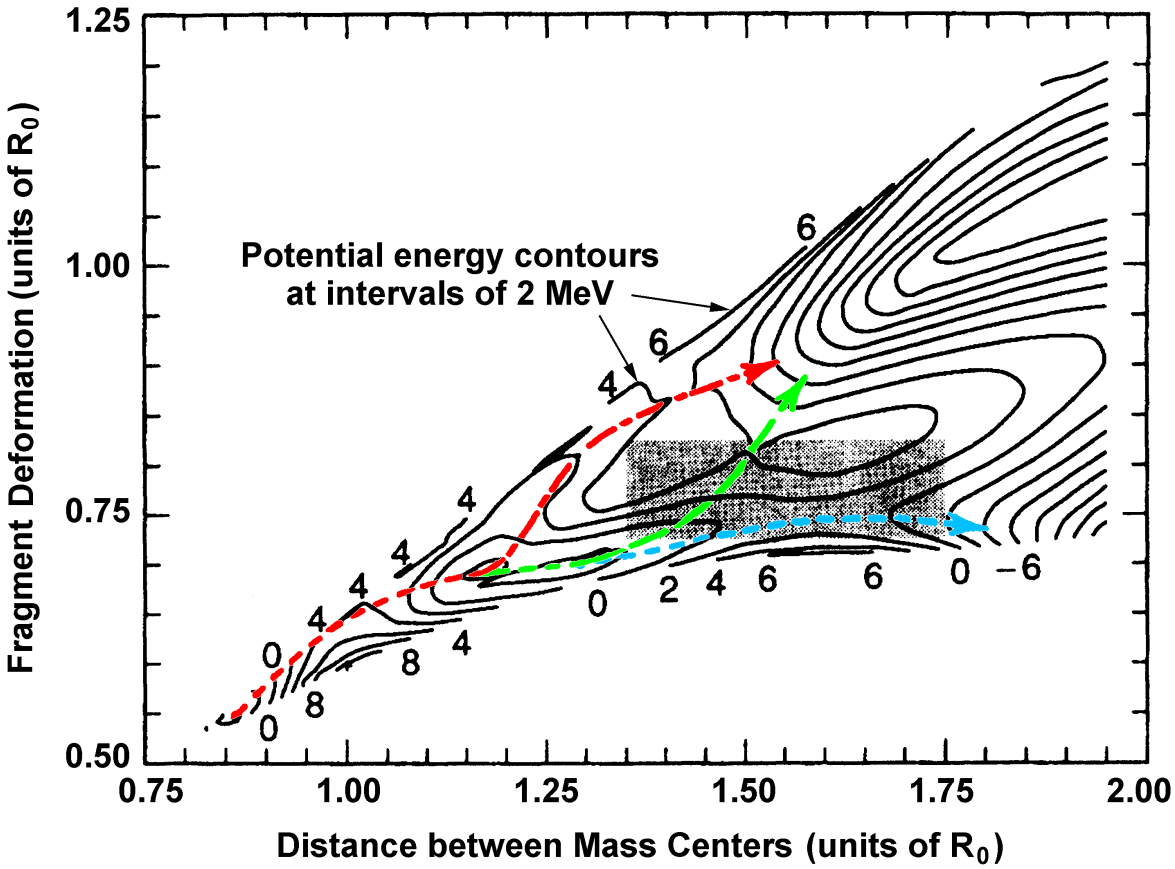

Figure 34. Calculated potential energy surface for ^{258}Fm. Note: This is taken from Ref. 35.

The plot of potential energy contours in the plane of the two variables, fragment deformation and distance between the mass centers of the two incipient fragments (elongation), is shown in Figure 34 for ^{258}Fm. The valleys leading from the deepest potential hole (the ground state) in the direction of increasing elongation are shown by red, green, and blue curves. A single valley (red curve) starts from the ground state and then branches at a secondary minimum. The upper branch in the diagram (red curve) moves in the direction of increasing fragment deformation. This may be termed the "traditional" path towards fission. The other branch (green curve) proceeds towards greater elongation before it again branches in front of a small potential hill. This hill (located at the coordinate x = 1.6, y = 0.75) separates two saddle points that lead to two well-separated valleys descending to separate scission points. One of these rejoins the final descent of the "traditional" path that results in very deformed fragments. The other leads to a scission point where the fragments are nearly spherical.

Calculations that included a third variable, the mass-asymmetry coordinate, were made for the shaded area of Figure 34. These show that when the potential energy is minimized for mass asymmetry, the saddle points for the green and blue curves have very similar heights. Furthermore, the deformed fragment path (green) is mass asymmetric, while the blue path is mass symmetric. These features of the potential energy surface explain why mass-symmetric and mass-asymmetric fission of ^{258}Fm have comparable yields.[35]

In Ref. 35, the behavior of the inertial parameter of the deforming nucleus is also studied. Because of the orbital motion of the individual nucleons and its continual rearrangement as the nucleus deforms, the inertia is much greater than that of irrotational hydrodynamic flow at small elongations. Some of this difference is maintained at greater deformations along the "traditional" path, but not on the new path towards spherical fragments. Guided by these considerations on the inertial parameter, Moller et al.[35] made estimates of the spontaneous fission half-lives of the isotopes of Fm and other heavy elements. These reproduce the neutron dependence with its strong maximum (so very different from the linear Z^2/A relation) that is such a notable feature of Figure 2.

Some examples of these calculations and comparisons with experimental spontaneous fission half-lives are shown in Figures 35 to 37. The calculated and experimental half-lives are shown for Cf, Fm, and No isotopes as a function of Z^2/A. Although there are differences of up to 5 or more orders of magnitude in absolute values between theory and experiment (which may be due to error in the calculated ground state energies), the trends of the data are well reproduced by the new theory that takes shell effects fully into account right up to the scission point. The plot against Z^2/A reveals the dramatic effect that the neutron number has on spontaneous fission half-lives (as well as on the other fission properties we have mentioned above). Above $N = 158$ a new valley to the scission point is opened up by the proximity of the ^{132}Sn fission product and this new valley lowers the half-life dramatically. The valley leading to the more conventional asymmetric mass division of the actinides gives half-lives 11 to 13 orders of magnitude greater than those of the new valley at the scission point magic number of 164 neutrons.

With modern super-computer capabilities, even more comprehensive searches of the nuclear energy vs. deformation surface are being explored.[36,37]

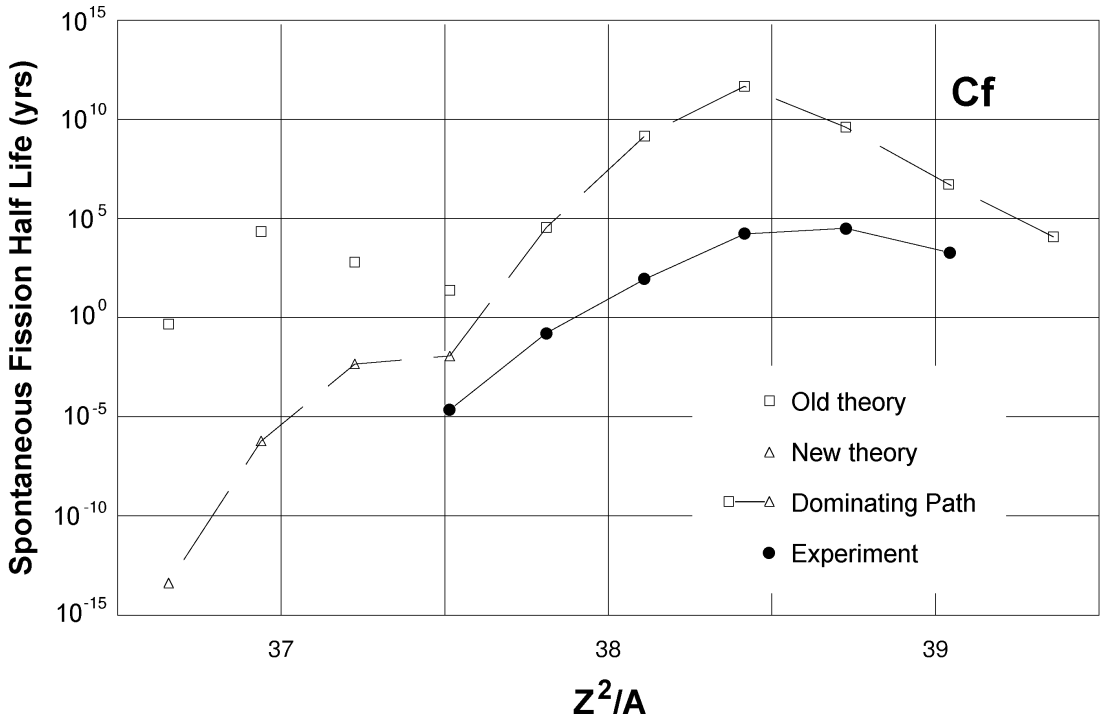

Figure 35. Experimental vs. calculated fission half-lives for Cf. Note: This is taken from Ref. 35.

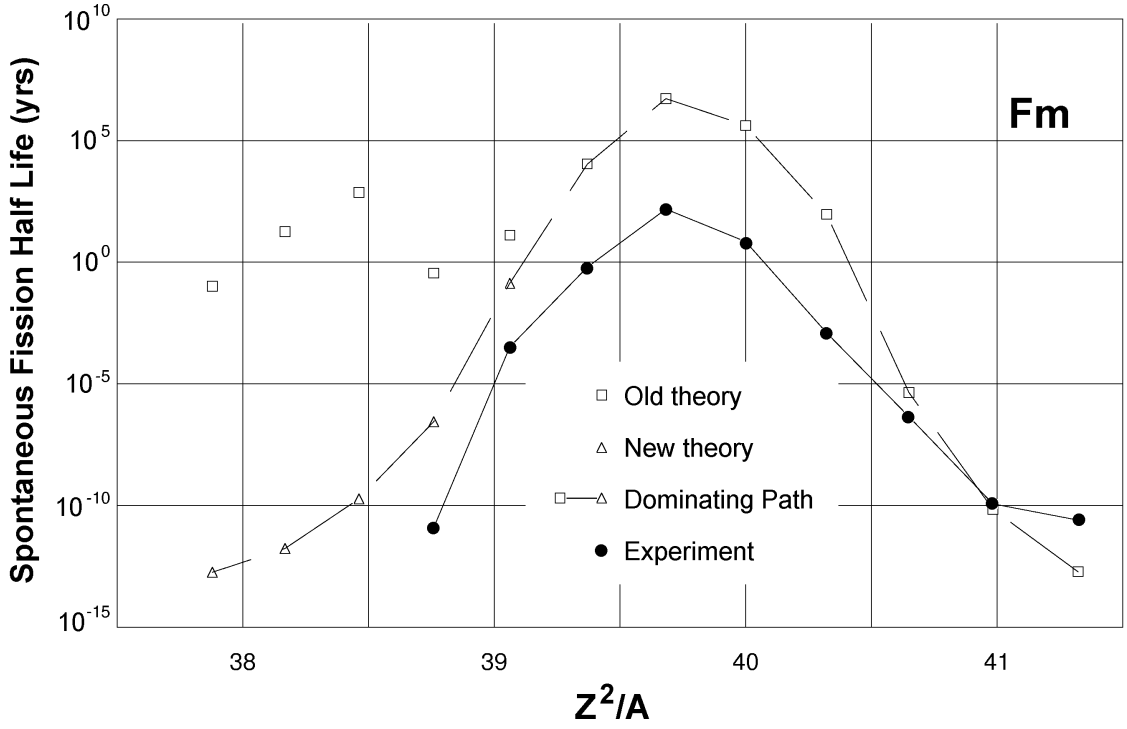

Figure 36. Experimental vs. calculated fission half-lives for Fm. Note: This is taken from Ref. 35.

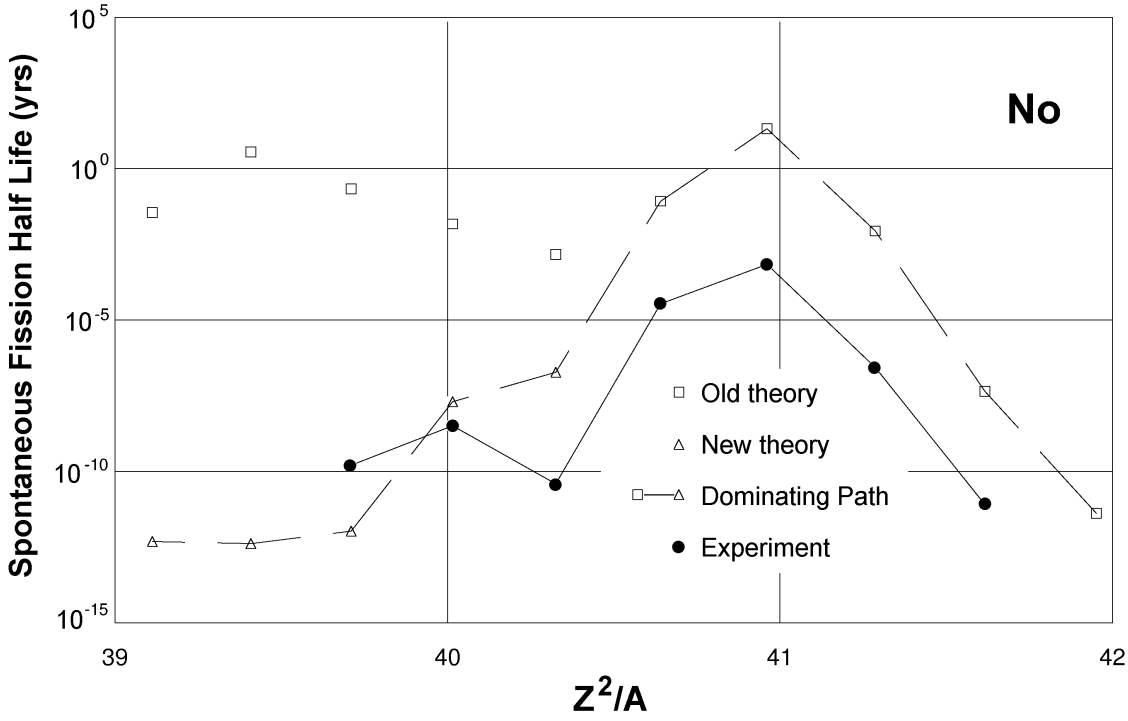

Figure 37. Experimental vs. calculated fission half-lives for No. Note: This is taken from Ref. 35.

X. Calculation Capability

With barrier parameters that result from analysis of all available cross-section data (as shown in previous diagrams) and with theoretical construction of transition state spectra at the barriers, it is possible to calculate barrier transmission coefficients, or the equivalent mean barrier widths. Hence from nuclear reaction theory we can calculate average fission cross sections with a fair degree of confidence. Some examples are shown below.

The first example is the fission cross section of ^{235}U. The ^{235}U (*d,p,f*)* and ^{234}U (*t,p,f*) reactions can be used to excite compound nucleus states of ^{236}U well below the neutron separation energy. With barrier heights obtained from the analysis of the data from these reactions, we can adjust the transition state spectra to fit the fast neutron fission cross section. ^{235}U has a very low energy spin isomer at only 78 eV with a half-life of 25 min. Because of the different spins (^{235}U ground is $J^{\pi} = 7/2^{-}$ while the isomer is $J^{\pi} = 1/2^{+}$) a quite different range of spin and parity is excited in the compound nucleus especially at low neutron energies. Thus, the cross sections shown as ratios of capture cross section to fission cross section can be quite different even though the basic barrier heights are the same. The comparative cross sections are shown in Figure 38.

The second example is the fission cross section of ^{233}U ($J^{\pi} = 5/2^{+}$). Using essentially the same barrier parameters as ^{235}U, we calculate the cross section shown in Figure 39 in comparison with the experimental data. This cross section is greater than that of ^{235}U, largely because the neutron separation energy is greater.

In Figure 40 we show the calculated fission cross section of ^{237}U (half-life of 5 days) together with the very limited and very uncertain data. Like the isomer of ^{235}U this nucleus has $J^{\pi} = 1/2^{+}$.

Finally, in Figure 41, we show the calculated and measured cross sections of ^{239}Pu which has $J^{\pi} = 1/2^{+}$. From Figures 22 and 23, the inner barrier is about the same as for ^{235}U but the outer barrier is about 0.5 MeV lower. Also, ^{239}Pu has nearly the same neutron separation energy as ^{235}U. Using these parameters, the calculated cross section of ^{239}Pu agrees quite well with the data, and we note that because of the spin-parity properties, the low energy neutron cross section is somewhat suppressed, like ^{235}U (isomer) and ^{237}U compared with ^{235}U (ground) and ^{233}U.

* In this nomenclature, a deuterium nucleus is absorbed, a proton is emitted, and the resulting nuclide fissions.

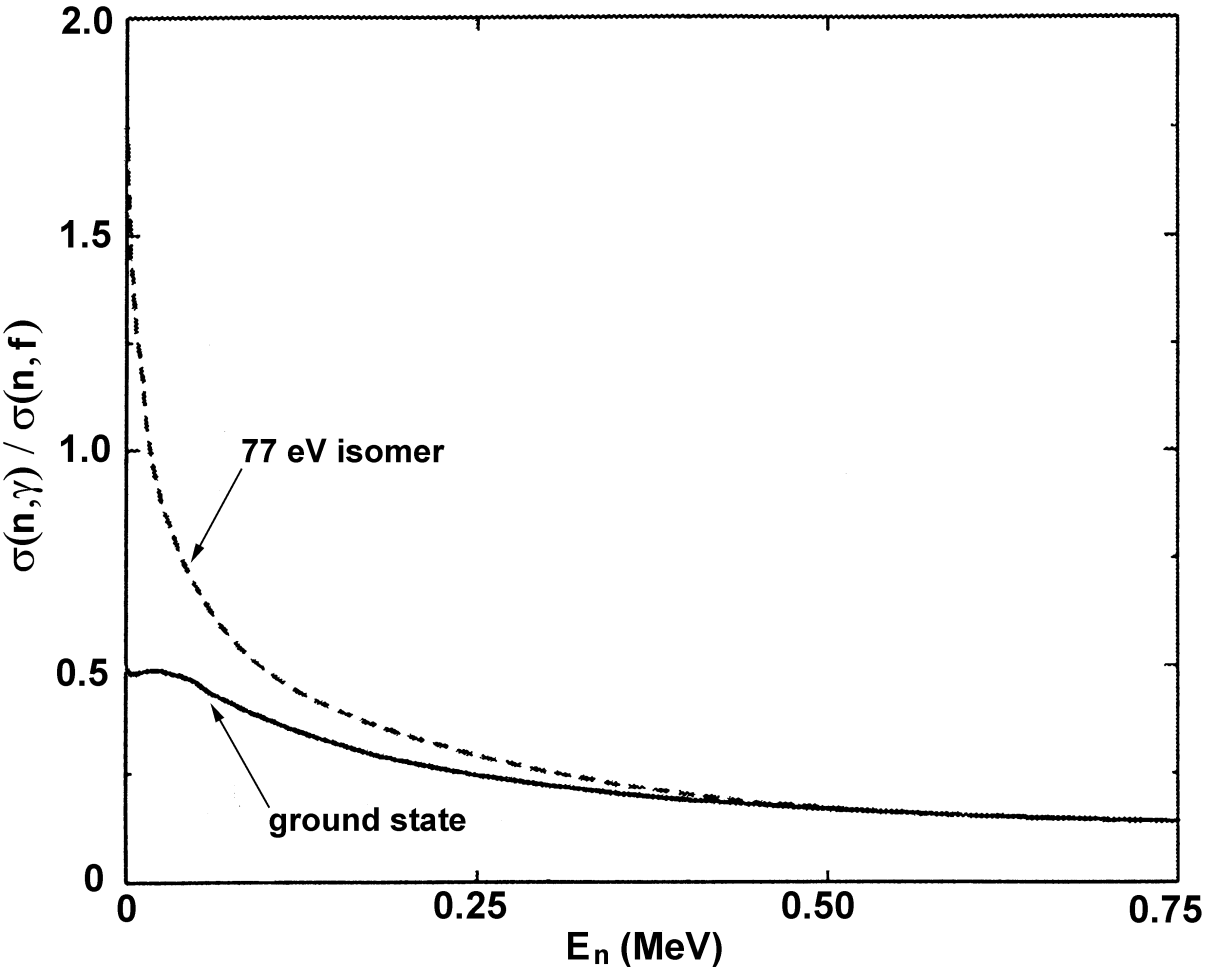

Figure 38. Ratio of capture to fission cross sections calculated for the ^{235}U ground state and for its isomer. Note: This is Fig. 8 of Ref. 38.

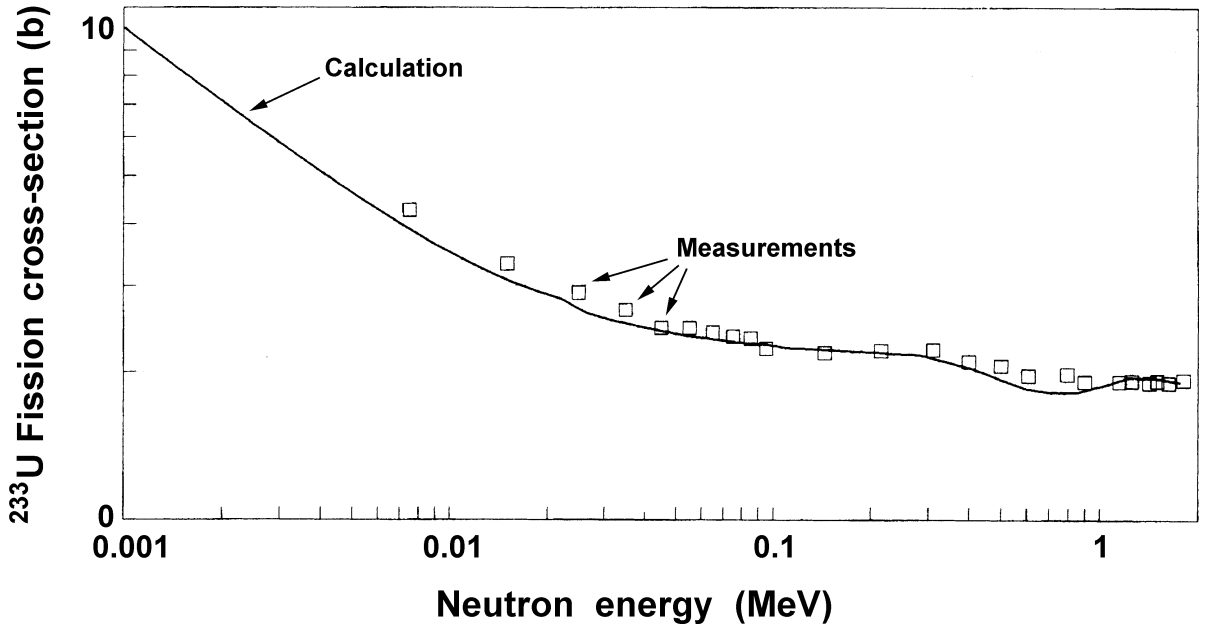

Figure 39. Calculated fission cross section of ^{233}U compared with experimental data. Note: This is adapted from Ref. 38.

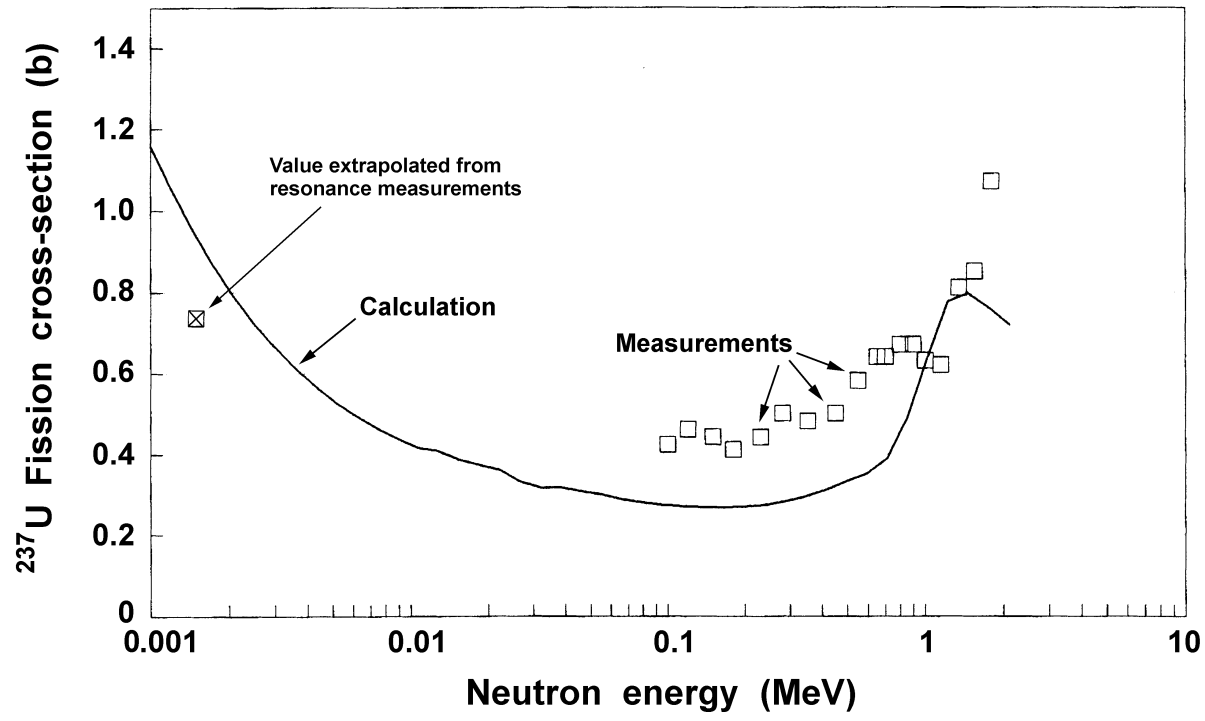

Figure 40. Calculated fission cross section of ^{237}U compared with experimental data. Note: This is adapted from Ref. 38.

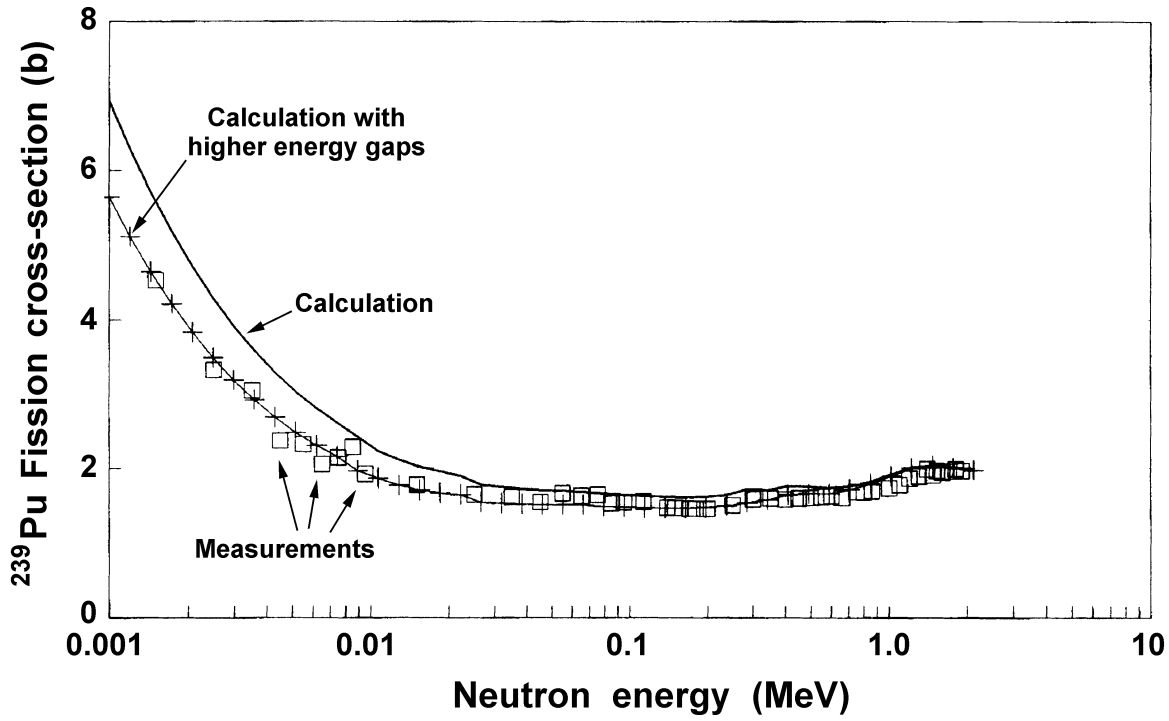

Figure 41. Calculated fission cross section of ^{239}Pu compared with experimental data. Note: This is from Ref. 38. The upper curve is based on the transition state spectrum used for fitting the cross section of ^{235}U. The lower curve employs slightly higher energy gaps in this spectrum.

XI. Conclusions

1) The dependence of Appendix A on Vandenbosch and Seaborg[3] is totally outmoded. The model is largely empirical, and when it is not, it is based on liquid-drop model concepts that only give global outlines of the fission process.

2) Many of the nuclides listed in Appendix A do not require a theoretical estimate of barrier height. Data are available from a wide range of reaction processes that can be analyzed to give barrier parameter information. Interpolation or extrapolation with the aid of modern fission barrier theory can fill the gaps. With modern supercomputers, alternative routes ('saddle points') to fission through the multidimensional deformation landscape of the nucleus can be explored theoretically.

3) With our current understanding of the compound nucleus (i.e., level densities, radiation widths, neutron strength functions, and statistics – "quantum chaos") and the fission process, we can compute average* neutron fission cross sections from the keV region upwards. The previous examples of neutron fission cross sections calculated using current fission models demonstrate the power of these models. We also have the potential to compute (using Monte Carlo techniques) the probability of thermal neutron fission cross sections lying within a certain range, or, alternatively, the probability of the ratio of thermal to capture cross sections lying in a certain range.

4) All of the above theory is continually being improved. Coupled with the available experimental data, we can make confident estimates of fission and capture cross sections over a wide range of energies for nearly all of the nuclides considered in Appendix A of the Standard that is currently under revision.

* In this discussion, "average" means the average value over all the resonances within a given energy interval.

References

1. *American National Standard for Nuclear Criticality Safety in Operations with Fissionable Materials Outside Reactors*, ANSI/ANS–8.1–1998, American Nuclear Society (September 1998).
2. *American National Standard for Nuclear Criticality Control of Special Actinide Elements*, ANSI/ANS–8.15–1981, American Nuclear Society (November 1981).
3. R. Vandenbosch and G. T. Seaborg, "Considerations on the Probability of Nuclear Fission," *The Physical Review,* **110** (2), 507–513 (April 1958).
4. C. F. von Weizsäcker, "Zur Theorie der Kernmassen," *Zeitschrift für Physik* **96**, 431 (1935).
5. L. Meitner and O. R. Frisch, "Disintegration of Uranium by Neutrons: a New Type of Nuclear Reaction," *Nature,* **143**, 239 (February 1939).
6. O. Hahn and F. Strassmann, "Über den Nachweis und das Verhalten der bei der Bestrahlung des Urans mittels Neutronen entstehenden Erdalkalimetalle," *Die Naturwissenschaften,* **27**, 11–15 (1939).
7. N. Bohr and J. A. Wheeler, "The Mechanism of Nuclear Fission," *The Physical Review,* **56** (2), 426 (September 1939).
8. S. Frankel and N. Metropolis, "Calculations in the Liquid-Drop Model of Fission," *The Physical Review,* **72** (10), 914–925 (November 1947).
9. G. T. Seaborg, "Activation Energy for Fission," *The Physical Review,* **88** (4), 1429 (November 1952).
10. G. T. Seaborg, "Some Comments on the Mechanism of Fission," *The Physical Review,* **85**, 157 (January 1952).
11. N. E. Holden and D. C. Hoffman, "Spontaneous Fission Half-Lives for Ground-State Nuclides," *Pure and Applied Chemistry*, **72**, 1525–1562 (2000).
12. R. Vandenbosch and J. Huizenga, *Nuclear Fission* (Academic Press, New York, 1973).
13. A. Bohr and B. R. Mottelson, "Single-Particle Motion," *Nuclear Structure* (W. A. Benjamin, New York), Volume I, p. 168 (1969).
14. M. G. Mayer and J. Hans D. Jensen, *Elementary Theory of Nuclear Shell Structure* (John Wiley & Sons, New York), p. 58 (1955).

15. C. Gustafson, I. L. Lamm, B. Nilsson, and S. G. Nilsson, "Nuclear Deformabilities in the Rare-Earth and Actinide Regions with Excursions off the Stability Line and into the Super-Heavy Region," *Arkiv för Fysik,* **36** (69), 613 (November 1967).

16. A. Bohr, "On the Theory of Nuclear Fission," in *Proceedings of the International Conference on the Peaceful Uses of Atomic Energy, Geneva, August 1955*, Volume 2, pp. 151–154, 220–224 (1956).

17. S. Bjornholm and J. E. Lynn, "The Double-Humped Fission Barrier," *Reviews of Modern Physics,* **52** (4), 725 (October 1980).

18. G. N. Flerov and S. M. Polikanov, "Nuclear Fission," *Comptes Rendus du Congrès International de Physique Nucléaire, Paris, July 1964,* Volume I, p. 407 (1964).

19. W. Kolar and K. H. Böckhoff, "Resonance Parameters of ^{240}Pu, Part I – Neutron Widths," *Journal of Nuclear Energy,* **22** (1), 299–315 (January 1968).

20. E. Migneco and J. P. Theobald, "Resonance Grouping Structure in Neutron Induced Subthreshold Fission of ^{240}Pu," *Nuclear Physics,* **A112,** 603–608 (May 1968).

21. V. M. Strutinsky, "Microscopic Calculations of the Nucleon Shell Effects in the Deformation Energy of Nuclei," *Arkiv För Fysik,* **36,** 629 (1967).

22. V. M. Strutinsky, "Shell Effects in Nuclear Masses and Deformation Energies," *Nuclear Physics,* **A95,** 420–442 (March 1967).

23. H. C. Pauli and T. Ledergerber, "The Dynamics of Fission in the Subbarrier Region of Deformation," *Proceedings of the Third IAEA Symposium on the Physics and Chemistry of Fission, Rochester, New York, August 1973,* Volume I, p. 463 (1974).

24. M. Brack et al., "Funny Hills: The Shell-Correction Approach to Nuclear Shell Effects and Its Applications to the Fission Process," *Reviews of Modern Physics,* **44** (2), 320 (April 1972).

25. J. R. Nix, "Calculation of Fission Barriers for Heavy and Superheavy Nuclei," *Annual Review of Nuclear Science,* **22,** 65 (1972).

26. H. J. Specht, J. Weber, E. Konecny, and D. Heunemann, "Identification of a Rotational Band in the ^{240}Pu Fission Isomer," *Physics Letters,* **41B** (1), 43 (September 1972).

27. D. L. Hill and J. A. Wheeler, "Nuclear Constitution and the Interpretation of Fission Phenomena," *The Physical Review,* **89** (5), 1102 (March 1953).

28. S. Bjornholm and V. M. Strutinsky, "Intermediate States in Fission," *Nuclear Physics,* **A136,** 1–24 (October 1969).

29. B. B. Back et al., "Fission of Odd-A and Doubly Odd Actinide Nuclei Induced by Direct Reactions," *Physical Review C,* **10** (5), 1948–1965 (November 1974).

30. S. Aberg et al., "Shell Structure at High Spins," *Proceedings of an International Symposium on Physics and Chemistry of Fission, Jülich, May 1979,* Volume I, p. 348 (1980).

31. J. E. Lynn, "The Topography of the Nuclear Fission Barrier," *Pramăna – Journal of Physics,* **33** (1), 69 (July 1989).

32. G. D. James, J. E. Lynn, and L. G. Earwaker, "Nuclear Spectroscopy of Highly Deformed ^{231}Th," *Nuclear Physics,* **A189** (2), 225–249 (July 1972).

33. J. Blons et al., "On the Existence of Triple-Humped Fission Barriers in ^{231,233}Th," *Nuclear Physics,* **A414,** 1 (February 1984).

34. S. E. Larsson and G. Leander, "Fission Barriers for Heavy Elements with Quadrupole, Hexadecapole and Axially Asymmetric Distortions Taken into Account Simultaneously," *Proceedings of the Third IAEA Symposium on the Physics and Chemistry of Fission, Rochester, New York, August 1973,* Volume I, p. 177 (1974).

35. P. Möller, J. R. Nix, and W. J. Swiatecki, "New Developments in the Calculation of Heavy-Element Fission Barriers," *Nuclear Physics,* **A492** (3), 349–387 (February 1989).

36. E. K. Hulet et al., "Bimodal Symmetric Fission Observed in the Heaviest Elements," *Physical Review Letters*, **56** (4), 313–316 (January 1986).

37. P. Möller, D. G. Madland, A. J. Sierk, and A. Iwamoto, "Nuclear Fission Modes and Fragment Mass Asymmetries in a Five-Dimensional Deformation Space," *Nature*, **409**, 785–790 (February 2001).

38. J. E. Lynn and A. C. Hayes, "Theoretical Evaluations of the Fission Cross Section of the 77 ev Isomer of ^{235}U," *Physical Review C*, **67**, pp. 014607-1–10 (January 2003).

Addendum

We list here all the papers referenced in Vandenbosch and Seaborg,[3] the key paper for Appendix A of the Standard, with brief notes on the information used in Ref. 3.

1. *Bohr and Wheeler, Phys. Rev.* ***56****, 426 (1939)*. Key reference to liquid-drop model of fission with emphasis on importance of Z^2/A parameter. (This paper discusses the barrier height problem.)
2. *Huizenga and Duffield, Phys. Rev.* ***88****, 959 (1952)*. Inferred in Ref. 3 that Z^2/A is used to determine relative tendency for thermal-neutron induced fission. It is not! Only the neutron binding energy is used here. (This paper discusses the barrier height problem.)
3. *Seaborg, Phys. Rev.* ***88****, 1429 (1952)*. Reference for relationship of spontaneous fission half-life to Z^2/A used in Ref. 3. (This paper was used to calculate barrier heights in Ref. 3).
4. *Huizenga, Argonne National Laboratory Report, ANL-5150 (1953)*. This draws attention to the correlation of fast neutron (3 MeV) fission cross sections to Z^2/A. This is well-above barrier cross-section data, but is indicative of relative barrier height. Not further used in Ref. 3.
5. *Batzel, University of California Radiation Lab. Report UCRL-4303 (1954)*. Similar to *(4)*. Describes application and test with 340 MeV proton spallation reactions.
6. *Jackson, Proc. Symp. on Physics of Fission, Chalk River, Report CRP-642-A (1956).* Similar to *(4)* and *(5)*. Also describes correlation of fast neutron fission cross sections with difference between fission barrier and neutron binding energy.
7. *Huizenga, Gindler, and Duffield, Phys. Rev.* ***95****, 1009 (1954)*. Gives photofission yield (relative to ^{238}U) for betatron energies of 17 and 20 MeV (maximum photon energies well above fission barrier). Shows empirical correlation with Z^2/A.
8. *Huizenga, Proc. Int. Conf. on Peaceful Uses of Atomic Energy, vol. 2, p. 208 (United Nations, New York, 1956).* Reparametrizes the Frankel and Metropolis formula to reproduce the ^{238}U spontaneous fission half-life. The coefficient for dependence on barrier height is assumed constant for all heavy nuclides. (This paper discusses the barrier height problem.)

9. *Glass, Carr, Cobble, and Seaborg, Phys. Rev.* ***104****, 434 (1956)*. Describes spallation-fission competition following bombardment by 20-50 MeV He ions. Average neutron width to fission width ratios extracted at high excitation energies.

10. *Vandenbosch et al., Phys. Rev.* ***111****, 1358 (1958)*. Similar to *(9)*. Also increasing mass symmetry of fission product distribution observed at higher energies.

11. *Vandenbosch, Ph.D. thesis, University of California Radiation Lab. Report UCRL-3858 (1957)*. Adds more detail to *(10)*.

12. *Frankel and Metropolis, Phys. Rev.* ***72****, 914 (1947)*. Numerical calculations on liquid-drop model of fission. Gives barrier heights as function of Z^2/A, and barrier penetrability as function of excitation energy for case of ^{238}U. Key reference for *(3)* and Ref. 3. (This paper was used to calculate barrier heights in Ref. 3).

13. *Swiatecki, Phys. Rev.* ***101****, 97 (1956)*. Alternative approach, based somewhat more securely on liquid-drop model, for obtaining barrier heights from Z^2/A. Not further referenced or used in Ref. 3. (This paper discusses the barrier height problem.)

14. *Seaborg, Phys. Rev.* ***85****, 571 (1958)*. Draws attention to empirical relationship between spontaneous fission half-life and Z^2/A. Key reference for *(3)* and Ref. 3. (This paper was used to calculate barrier heights in Ref. 3).

15. *Whitehouse and Galbraith, Nature* ***169****, 494 (1952)*. Draws attention to empirical relationship between spontaneous fission half-life and Z^2/A. (This paper discusses the barrier height problem.)

16. *Ghiorso et al., Phys. Rev.* ***87****, 163 (1952)*. Adds extra spontaneous fission half-lives to data base. Incorporated in Ref. 3. (This paper was used to calculate barrier heights in Ref. 3).

17. Footnote about terminology in relation to *(3)*.

18. *Hughes and Harvey, Neutron Cross Sections, Brookhaven National Laboratory Report, BNL-325 (1955)*. Compilation of cross sections used for construction of Table I in Ref. 3. (This paper was used to calculate barrier heights in Ref. 3).

19. *Stokes, Boyer, and Northrop, Bull. Am. Phys. Soc. Ser. II,* ***2****, 207 (1957)*. Reference to brand new experimental method for determining fission probability below the neutron binding energy. This has been greatly developed since 1957 and some experimental results are shown in section VIII of the present report. (This paper discusses the barrier height problem.)

20. *Stokes, Boyer, and Northrop, private communication*. Reports preliminary results on ^{235}U which were roughly in agreement with conclusions of Ref. 3. Otherwise little impact on conclusions of Ref. 3. (This paper discusses the barrier height problem.)

21. *Huizenga, Phys. Rev.* ***94****, 158 (1954)*. Points out that evidence already exists for more complicated dependence of spontaneous fission half-life on Z^2/A. This fact is not used in Ref. 3. (This paper discusses the barrier height problem.)

22. *Ghiorso, Proc. Int. Conf. on Peaceful Uses of Atomic Energy, vol.7, p.15 (United Nations, New York, 1956)*. Notes change in spontaneous fission rate for neutron number > 152. (This paper discusses the barrier height problem.)

23. *Swiatecki, Phys. Rev.* ***100****, 937 (1955)*. Discusses deviations of spontaneous fission half-lives from simple Seaborg relationship. Not used in Ref. 3. (This paper discusses the barrier height problem.)

24. *Harvey et al., Phys. Rev.* ***104****, 1315 (1956)*. Discusses experimental techniques for (α,4n) reactions.

25. *Appendix II of (9)*. Deduction of branching ratios in (α,4n) reactions.

26. *John, Phys. Rev.* ***103****, 704 (1956)*. Information on total cross section for (α,4n) reactions.

27. *Fujimoto and Yamaguchi, Prog. Theor. Phys. Japan* ***5****, 76 (1950)*. Theoretical estimation of neutron to fission width ratio at high excitation energies.

28. *Hyde and Seaborg, Handbuch der Physik, Vol. 39*. Reference for table of neutron binding energies.

29. *Meadows, Phys. Rev.* ***98****, 744 (1955)*. Discusses level densities in relation to (p,α) and other proton reactions.

30. *Lindner and Osborne, Phys. Rev.* ***102****, 378 (1956)*. Experiments with 340 MeV proton spallation reactions. Finds neutron to fission width ratio essentially independent of excitation energy.

31. *Allen and Henkel. Review of fast neutron (10 keV to 10 MeV) reactions*. Gives estimates of neutron to fission width ratio at excitation energies of 10 MeV.

Los Alamos NM 87545